

Dense Water Formation on the Icelandic Shelf and Its Contribution to the North Icelandic Jet

 Yarisbel Garcia-Quintana¹ , Nathan Grivault¹ , Xianmin Hu¹ , and Paul G. Myers¹ 
¹Department of Earth and Atmospheric Sciences, University of Alberta, Edmonton, AB, Canada

Key Points:

- Observations and model data show that overflow waters are formed on the northwest Icelandic shelf from the transformation of Atlantic inflow
- A dense plume is generated from this transformation through shelf convection linked to winter heat loss northwest of Iceland
- Waters from the modeled plume cascade north of Iceland feeding into the North Icelandic Jet contributing up to 21% of its lightest component

Supporting Information:

Supporting Information may be found in the online version of this article.

Correspondence to:

 Y. Garcia-Quintana,
yarisbel@ualberta.ca

Citation:

 Garcia-Quintana, Y., Grivault, N., Hu, X., & Myers, P. G. (2021). Dense water formation on the Icelandic shelf and its contribution to the North Icelandic Jet. *Journal of Geophysical Research: Oceans*, 126, e2020JC016951. <https://doi.org/10.1029/2020JC016951>

Received 6 NOV 2020

Accepted 19 JUL 2021

Abstract The North Icelandic Jet (NIJ) is the densest component of the Denmark Strait Overflow Water, feeding the abyssal limb of the Atlantic Meridional Overturning Circulation. Here, by using observational and numerical model data, we explore the formation of overflow water on the Icelandic shelf, the mechanisms involved, and its potential contribution to the NIJ. The sparse observational data on the western Icelandic shelf for the month of February shows top-to-bottom mixing on the shelf, distinct and well separated from the dense water offshore, with densities larger than 27.8 kg/m^3 in some years. Using a 1-D mixing model and winter heat flux reanalysis, we suggest that waters with densities exceeding 27.8 kg/m^3 are likely to be formed on the shelf in most years by the end of winter. High-resolution numerical model data shows that the transformation of the Atlantic inflow along the northwest Icelandic shelf generates a dense plume whose waters feed into the NIJ. The bulk of the plume cascades down-slope north of Iceland, funneled through deep cross-shelf troughs, with some cascading occurring west of Iceland as well. During years of strong cascading events (2008, 2013, and 2016), the modeled dense plume potentially feeds up to 21% of the NIJ transport at the Siglunes and Kögur sections. Back-tracked Lagrangian particle trajectories confirm that the western Icelandic shelf is a source of the NIJ. The dense plume transport and variability are found to be dependent on the total oceanic heat loss west of Iceland and along Denmark Strait.

Plain Language Summary Ocean currents distribute heat, nutrients, and gases. In the North Atlantic Ocean, through atmosphere-ocean interaction, northward-flowing surface warm waters lose heat as they approach sub-polar latitudes. Consequently, they get heavier and sink to greater depths. During this sinking process, known as deep convection, the ocean's intermediate and deep waters are ventilated, providing them with nutrients and gases. Simultaneously, the heat released into the atmosphere directly moderates the local climate. Deep convection, which plays a crucial role in the Earth's climate, is known to occur in the Nordic Seas, where southward-flowing currents carrying dense bottom waters are formed. The North Icelandic Jet (NIJ), suggested to be formed through deep convection, carries the heaviest waters formed in the Nordic Seas. In our study, by using model and observational data, we found that during the winters of 2008, 2013, and 2016 up to 21% of the lightest component of the NIJ comes from shelf convection occurring northwest of Iceland, where the continental shelf is not deeper than 250 m. These findings contribute to improving our understanding of the source waters of the NIJ.

1. Introduction

The Denmark Strait Overflow Water (DSOW) is the largest dense water plume from the Nordic Seas that feeds the lower limb of the Atlantic Meridional Overturning Circulation. The transport of the DSOW has been estimated to be around 3–3.5 Sv ($1 \text{ Sv} = 10^6 \text{ m}^3/\text{s}$) (Harden et al., 2016; Jochumsen et al., 2015, 2017; Våge et al., 2013). Its upstream sources, however, are still a topic of study (Huang et al., 2019; Pickart et al., 2017; Våge et al., 2011, 2013, 2015). Its primary source was commonly thought to be the East Greenland Current (EGC) (Figure 1). However, the North Icelandic Jet (NIJ) (Figure 1), a recently discovered current (Jonsson & Valdimarsson, 2004) that flows along the continental slope of Iceland toward Denmark Strait, has been argued to be the source for the densest component of the DSOW (Mastropole et al., 2017). The NIJ transport has been estimated to be between 1 (Harden et al., 2016) and 1.4 Sv (Våge et al., 2013), approximately half of the total DSOW transport (Våge et al., 2011).

Initially, it was suggested that the NIJ was not an independent current, but rather a branch of the EGC that bifurcates upstream of Denmark Strait (Köhl et al., 2007). Käse et al. (2009) argued that, at times, the NIJ

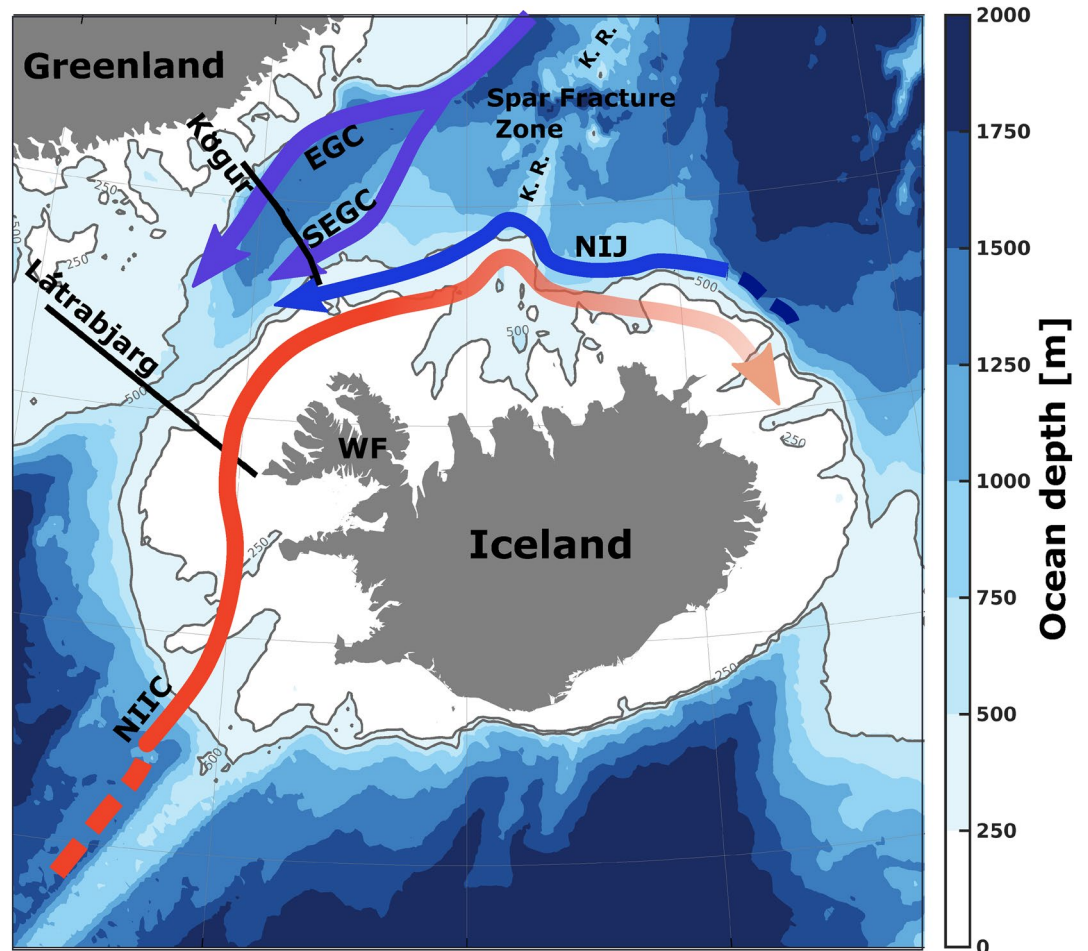


Figure 1. Schematic circulation in the vicinities of Iceland. The main currents shown and their acronyms are: shelfbreak East Greenland Current (EGC), separated East Greenland Current (SEGC), North Icelandic Irminger Current (NIIC) and the North Icelandic Jet (NIJ). The region northwest of Iceland known as the Westfjords is identified as WF. The Kolbeinsey Ridge is represented as K. R. in the map.

originates from a southward dense current flowing along the Jan Mayen Ridge. Köhl (2010), on the other hand, proposed that the source of the NIJ is linked to the magnitude of the cyclonic wind stress curl in the region. They claimed that when the curl is strong, the NIJ has its origin in the EGC. On the contrary, when the curl is weak the source of the NIJ is in the northern Iceland Sea, fed by an “offshoot of the weakening cyclonic circulation in the Iceland Sea.”

Våge et al. (2011) proposed that waters from the North Icelandic Irminger Current (NIIC) (Figure 1) are exchanged laterally (via eddies) with dense water transformed by means of deep convection in the interior of the Iceland Sea. Subsequently, the dense water sinks near the boundary to form the NIJ (Våge et al., 2011). However, Våge et al. (2015) pointed out that only a minor fraction (2%) of late-winter profiles (since 1980) from the north-central Iceland Sea, recorded a mixed layer dense enough to provide the waters that could feed the NIJ. They mentioned this could be due to an ongoing weakening of the convection in the Iceland Sea. However, a weakening of the NIJ transport strength has not been documented. In fact, it has already been suggested (Pickart et al., 2017; Våge et al., 2015) that the dense waters that feed the NIJ may not have been formed in the interior of the Iceland Sea.

Pickart et al. (2017) examined the relationship between the NIJ and the NIIC. They suggested that although interannual variability in salinity of the NIIC is in phase with that of the NIJ, the NIIC signal does not dictate that of the NIJ. Instead they propose that the salinity of the NIJ is in phase with the changes in evaporation minus precipitation over a region in the northwest of the Iceland Sea. Even though Pickart et al. (2017)

offer a different explanation, their findings makes one think that transformed waters from the NIIC could be feeding into the NIJ, even if such transformation does not occur within the Iceland Sea interior as previously proposed (Våge et al., 2011).

There are a series of recent modeling studies that looked at the potential link between NIIC and NIJ. Using a numerical model with a horizontal resolution of $1 / 20^\circ$ (VIKING20), a vertical grid of 46 z-levels and an off-line Lagrangian tool, Behrens et al. (2017) investigated the upstream sources of the DSO. They back-tracked the sources for the NIJ, suggesting that it originated mainly from the NIIC and from water mass transformation north of Iceland.

More recently, while exploring the pathways and water mass transformation of the NIIC in the Nordic Seas using two ocean circulation models, Ypma et al. (2019) showed that 0.2 Sv of the inflowing NIIC exits as DSO after getting transformed north of Iceland. Similarly, Saberi et al. (2020) in their detailed Lagrangian analysis of upstream sources of the DSO revealed a previously unknown pathway from south of Denmark Strait (for more details see Figure 14a from Saberi et al., 2020). A subset of the particles following the southern pathway were found to be shallower than 300 m and were present only during winter (Saberi et al., 2020). They hypothesized that this southern pathway could indicate a shortcut for NIIC waters that densify west of Iceland and turn around as they cascade over the Denmark Strait. They, however, did not explore the potential mechanism for the NIIC transformation.

Recently, by using mooring data from September 2011 to July 2013, on the Iceland slope (part of the Kögur section; see section position in Figure 1), Huang et al. (2019) determined three different scenarios of the NIJ. In order to establish a link between the timing of the dominant regime and the atmospheric forcing upstream of Denmark Strait, they looked into lagged correlations between the dominant NIJ regime with monthly heat fluxes and wind speed. For turbulent heat fluxes, two regions showed statistically significant correlations with the NIJ strength for a 2-month (positive) lag: one region located on the north slope of Iceland around the 1,000 m isobath (south side of the Spar Fracture zone; Figure 1), and a second region on the west/northwest corner of the Icelandic shelf (see Figures 12c, 13a and 13b of Huang et al., 2019). Strong turbulent heat flux in winter potentially causes the waters of the NIIC to densify west of Iceland, explaining the southern pathway of the DSO found by Saberi et al. (2020).

Observations do show evidence for the existence of dense water on the Iceland shelf (Figure 5 from Våge et al., 2015). It is currently believed that the dense (denser than 27.8 kg/m^3) bottom waters found on the Icelandic shelf have their origin in the dense (denser than 27.8 kg/m^3) layer that banks up along the north Icelandic slope (Jonsson & Valdimarsson, 2004; Pickart et al., 2017). According to De Jong et al. (2018), upslope motion of dense waters onto the shelf occurs along the northern Icelandic slope. While Jonsson and Valdimarsson (2004) suggested that the presence of dense waters on the Icelandic slope may be the result of a bottom Ekman layer generated by the NIJ, Pickart et al. (2017) suggested that it could rather be a compensating mechanism for offshore flow resulting from the interaction between the inshore front and the offshore front of the NIJ and the NIIC, respectively.

Our hypothesis, which derives from the connection among these findings (De Jong et al., 2018; Huang et al., 2019; Saberi et al., 2020; Våge et al., 2015; Ypma et al., 2019), is that the overflow waters observed on the Icelandic shelf are actually formed there through shelf convection. Formation of dense waters by cooling over continental shelf regions has been extensively studied (Canals et al., 2006, 2009; Ivanov et al., 2004; Killworth, 1983; Luneva et al., 2020; Palanques et al., 2006; Puig, 2017; Pusceddu et al., 2010; Vidal et al., 2009). Ivanov et al. (2004), for example, show a lengthy inventory of observed cases of water cascades around the World Ocean. Numerous regional modeling studies have also explored cascading events in the Arctic Ocean (Ivanov & Golovin, 2007; Ivanov et al., 2015; Luneva et al., 2020; Magaldi & Haine, 2015; Marson et al., 2017; Wobus et al., 2013).

There are four different stages to dense water cascading: (a) the pre-conditioning stage when dense water accumulates on the shelf and a density front is formed (convection reaches the bottom, forming a well-mixed water mass denser than the ambient waters); (b) the active stage, corresponding to the period when the leading edge of the dense water accelerates down-slope; (c) the main stage, which relates to a quasi-steady flow with a noticeable down-slope component; and the (d) final stage, when the descended water spreads isopycnically off the slope (Ivanov et al., 2004). Once formed, the dense water propagates mainly

along-slope due to Coriolis forcing and downslope as a bottom boundary current while mixing with the ambient waters en route.

The sea-floor topography is known to play an essential role in the path the dense waters follow (Chapman & Gawarkiewicz, 1995; Kämpf, 2005; Puig, 2017; Pusceddu et al., 2010). Numerous linear to curvilinear cross-shelf depressions (glacially eroded) incise the Icelandic continental shelf (Clark & Spagnolo, 2016). On the northern shelf, these troughs are known to be “deep, long, sinuous and distributive” (Clark & Spagnolo, 2016). These troughs along the northern continental Icelandic shelf have the potential to act as down-slope channels for dense waters.

Here, by using a high-resolution numerical model, we aim to explore the transformation of the Atlantic inflow along the Icelandic shelf and its link to the NIJ. In this study, we demonstrate that waters from the NIIC transform northwest (NW) of Iceland through winter-time shelf convection, generating a dense plume that feeds into the NIJ. After introducing the observational data set and the numerical model used in this manuscript in Section 2, we explore the existence of overflow waters on the Icelandic shelf from observations in Section 3. In Section 4, we investigate, from the model perspective, the evolution of the dense plume that results from the densification of NIIC waters west of Iceland. The pathways of the plume and its potential contribution to the NIJ are analyzed in Section 4. Section 5 offers the discussion of the main findings as well as the manuscript's conclusions.

2. Methods

2.1. Observations

Temperature and salinity profiles from 1929 to 2018, between 28° to 17°W and 64° to 67°N, used to explore the presence of overflow water on the continental Icelandic shelf (shallower than 250 m depth) were acquired through the International Council for the Exploration of the Sea database. However, the bulk of our study was made by analyzing the years from 2000 to 2018 as the numerical simulation used here covers the years from 2002–2018.

2.2. Ocean-Sea Ice Model

We used the Nucleus for European Modeling of the Ocean (NEMO) numerical framework version 3.4 (Madec & the NEMO team, 2008). The model uses the Louvain-la-Neuve LIM2 sea ice module (Fichefet & Maqueda, 1997). The configuration used is called *Arctic and Northern Hemisphere Atlantic* and has a 1 / 12° resolution, hence its acronym ANHA12 (Grivault et al., 2018; Hu et al., 2019). Within the Nordic Seas, the horizontal resolution is between 4 and 5 km (Figure 1 in Hu et al., 2018). ANHA12 has open boundaries at Bering Strait and at 20° south. The model configuration has 50 vertical z -levels, with the layer thickness smoothly increasing from 1.05 m at the surface to 453.13 m in the last level. Partial step is also enabled to better resolve the sea floor (Barnier et al., 2006). The simulation is integrated from January 1, 2002 to December 31, 2018. Initial and open boundary conditions (temperature, salinity, zonal and meridional horizontal velocities, and sea surface height [SSH]) are both obtained from *Global Ocean Reanalysis and Simulations* (GLORYS2v3) from Mercator Ocean (Masina et al., 2017). GLORYS2v3 is used for the open boundary conditions until the end of 2014, and the source is switched to GLORYS2v4 from the beginning of 2015. As GLORYS2v3 has been already spun up and ran for several years, this approach helps to reduce the model spin-up time allowing for the numerical experiment to have a shorter adjustment period. No temperature or salinity restoring is applied. The atmospheric forcing used comes from the *Canadian Meteorological Centre's Global Deterministic Prediction System* (GDPS) (Smith et al., 2014). GDPS provides 10 m surface wind, 2 m air temperature and specific humidity, downward long-wave and short-wave radiation fluxes and total precipitation. This data set has a temporal resolution of 1 h and a spatial resolution of 0.45° in longitude and 0.3° in latitude.

The Coordinated Ocean-ice Reference Experiments bulk formulae were applied to compute fluxes of heat, freshwater and momentum at the surface of the ocean (Large & Yeager, 2009). Sensible (Equation 1) and latent (Equation 2) turbulent heat fluxes are determined from the humidity, temperature, and velocity difference between the surface of the ocean and the overlying atmosphere. Positive values indicate a heat flux

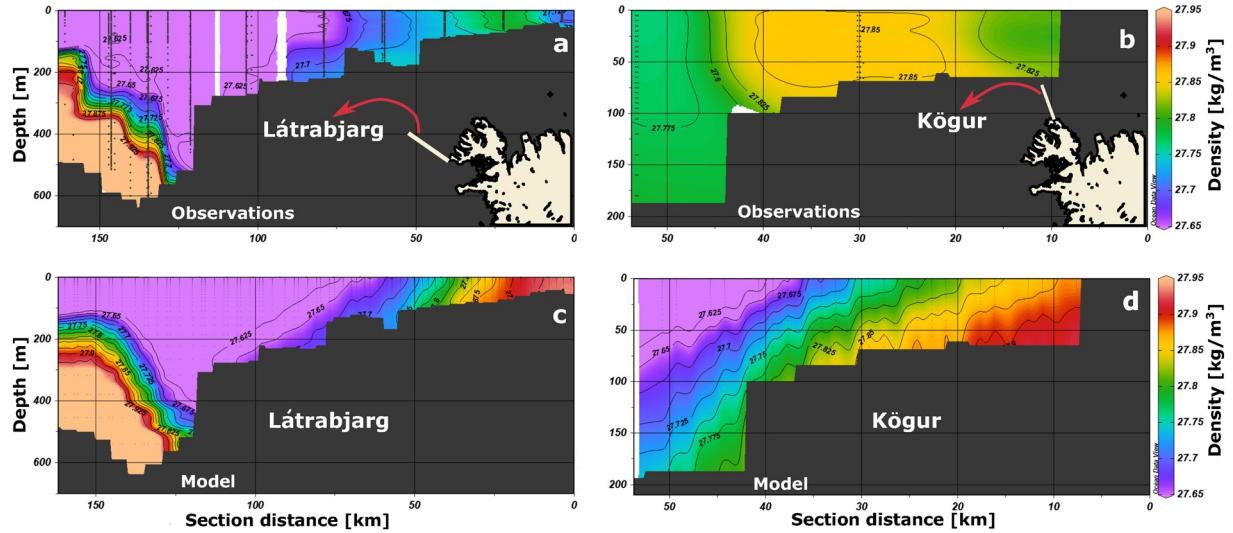


Figure 2. Observed and model density along the Látrabjarg (observations in (a), model in (c)) and the Kögur (observations in (b), model in (d)) sections during the month of February. In the case of the observations, the average considers the years when the density on the shelf was $\geq 27.8 \text{ kg/m}^3$: for the Látrabjarg section, the years 1983, 1984, 1988, 1997 were considered, and 2011, and for the Kögur section, the years 1984, 1988, 2004, and 2016. In the case of the model, we considered the period from 2004 to 2018. The exact position of the sections can be seen in the inset map on panel (a) (Látrabjarg) and (b) (Kögur).

from the atmosphere into the ocean, while negative values indicate heat transferred from the ocean into the atmosphere (heat loss).

$$\text{Sensible turbulent heat flux} = C \rho_{\text{air}} C_h (T_a - T_o) U_{ao} \quad (1)$$

$$\text{Latent turbulent heat flux} = \rho_{\text{air}} C_e L_v (q_a - q_o) U_{ao} \quad (2)$$

The variables in Equations 1 and 2 are as follows: C is the specific heat of air at $1000.5 \text{ J kg}^{-1} \text{ K}^{-1}$, ρ_{air} is the air density of 1.22 kg m^{-3} , T_o is the ocean surface temperature in Kelvin, T_a is the potential air temperature in Kelvin, L_v is the latent heat of vaporization ($2.5 \times 10^6 \text{ J kg}^{-1}$), q_o is the saturated specific humidity (kg kg^{-1}) at T_o , q_a is the specific humidity (kg kg^{-1}) of the air at 10 m height, U_{ao} is the relative wind speed (m/s) with respect to the surface ocean current, while C_h and C_e are sensible and latent transfer drag coefficients, respectively (for more details see Large & Yeager, 2009).

3. Observed Dense Water Formation on the NW Icelandic Shelf

A total of 1,202 winter profiles sampled along the sections within the region of interest (Faxaflói, Látrabjarg, Kögur, and Siglunes), between 1980 and 2018, were analyzed. Figures 2a and 2b show the averaged density for the month of February along the sections Látrabjarg and Kögur, respectively, averaged over the years when the densities are greater than 27.8 kg/m^3 (upper limit of overflow water). According to the observational data used here, this occurred in the case of Látrabjarg in 1983, 1984, 1988, 1997, and 2011, and in the case of the Kögur section in 1984, 1988, 2004, and 2016. In both cases, top-to-bottom mixing of dense waters on the shelf in about 100 m of water can be observed, specifically around the inshore stations in both sections. We compared the observed (Figures 2a and 2b) and modeled (Figures 2c and 2d) mean February density at Látrabjarg and Kögur sections. The comparison shows that even when the model is denser (most likely due to salinity bias), it simulates nicely the overall structure of the water column along both sections with dense water on the shelf in winter. Therefore we can use the model to examine mechanisms and pathways by which this dense water is transported off the shelf.

Note that the observational profiles shown in Figure 2 correspond to the month of February, and thus more heat loss through February and the rest of winter is still expected. What is more, the position of both sections (inset map in Figure 2) coincides with a region of intense turbulent heat flux which is the strongest along a band that extends through Denmark Strait to the northern Irminger Sea (Huang et al., 2019).

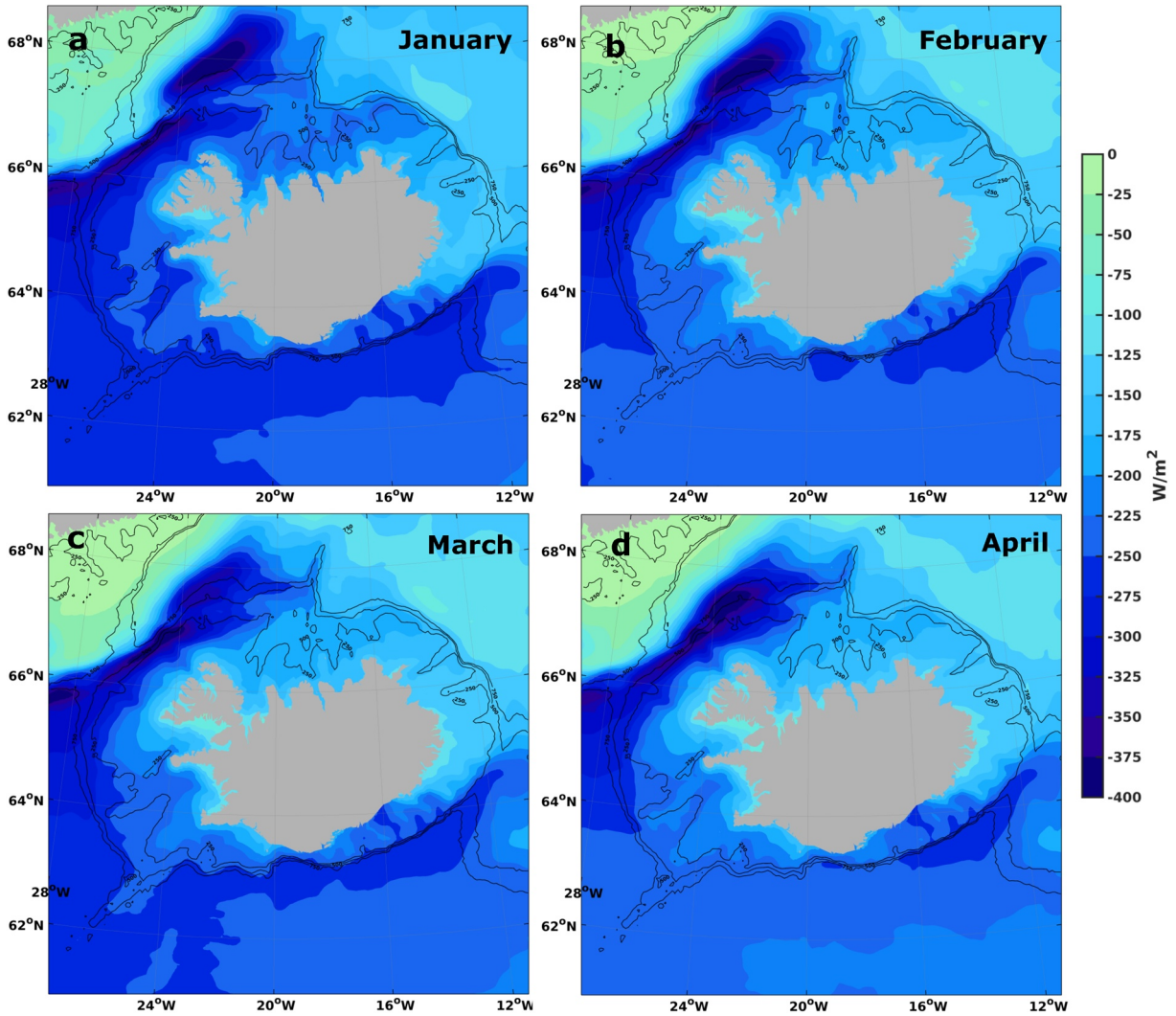


Figure 3. Mean net surface oceanic heat loss for (a) January, (b) February, (c) March, and (d) April taken from the model output, computed based on the CGRF reforecast fields and the bulk formula of Large and Yeager (2004), the averaging was done over the period 2002–2018. Negative values mean that the heat flux is from the ocean to the atmosphere (heat loss).

Figure 3 shows monthly average (2002–2018) net surface air-sea oceanic heat loss (indicated by negative values). We selected the months from January (Figure 5a) to April (Figure 3d) as during those months the heat loss is the strongest. The largest heat loss occurs along the west/northwest portion of the Icelandic shelf, which coincides with Huang et al. (2019). We examined other reanalysis products as well (not shown) and all show strong winter heat loss in this region.

Given the fact that observed data along the Látrabjarg and Kögur sections for the month of March is scarce, we estimate the mean density field for that month by using a simple 1-D mixing model. To do so, we consider only the years when dense water is seen on the NW Iceland shelf in February, but yet not dense enough (between 27.74 and 27.8 kg/m³) to contribute to the Denmark Strait overflow (Figures 4a and 4b). Considering these observations and assuming an idealized water column of 1 m² of area (A) we compute its heat content (HC):

$$HC = \rho * Cp * \int_0^z (T_z - T_{ref}) dz * A \quad (3)$$

where z is the depth, $\rho = 1,000 \text{ kg/m}^3$, T is the temperature from the observations (profiles which density on the shelf is between 27.74 and 27.8 kg/m³), $T_{ref} = 0 \text{ }^\circ\text{C}$ for simplicity and $Cp = 4000 \text{ J/kg/K}$. We then examine

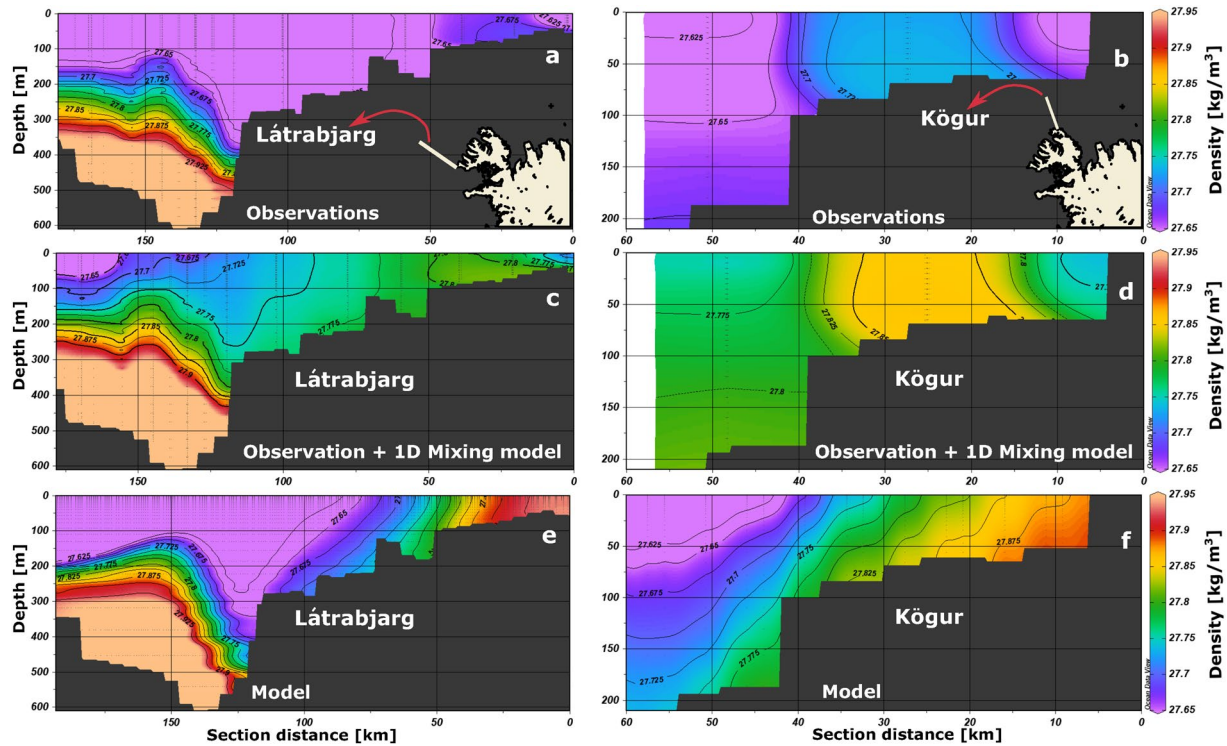


Figure 4. Observed (a and b) and 1D-mixing-model (c and d) density along the Látrabjarg and the Kögur sections. In the case of the observations (a and b), the average February is shown, considering the years between 2000 and 2018 when the density on the shelf for both sections was between 27.74 and 27.8 kg/m³. In the case of the 1D-mixing-model, (c and d) show the density field resulting from applying the February heat loss on the observations (shown in (a and b)). Average (2004–2018) modeled March, density is shown in panels (e and f). The exact position of the sections can be seen in the inset map on panel (a) (Látrabjarg) and (b) (Kögur).

through the simple 1-D mixing model if the heat loss during the month of March (Figure 2c) is sufficient to increase the density of the shelf waters over 27.8 kg/m³ during the remaining parts of winter (month of March) when observations are lacking.

Note that although a simple 1-D mixing model does not consider advection, it is likely that water parcels remain on the shelf for at least a month, and thus continue to densify. For example, considering that a typical velocity of the NIIC along the NW Iceland shelf during the winter months is of the order of 0.1 m/s (Pickart et al., 2017; Semper et al., 2019), over the course of a month water parcels in the region would thus travel only about 250 km along the Icelandic shelf.

The average net surface March winter heat loss in the region (NW Iceland shelf) is around 200 W/m² as shown in Figure 3c. This is a total heat loss of $\sim 5.184 \times 10^8$ J/m² over the month of March. Removing such heat loss from the February heat content estimated from the observed sections data (Figures 5a and 5b, in orange), and using Equation 3, we can roughly estimate the March heat content (Figures 5a and 5b, in blue). Using the estimated March heat content and reversing Equation 3 we compute the estimate March temperature (Figures 5c and 5d, in blue), and assuming that the salinity stays the same, compute an estimated March density (Figures 5e and 5f, in blue). We thus expect an underestimation of density as salinity tends to increase due to wind-induced evaporation from strong winds in winter. Thus, given typical winter air-sea fluxes, when the dense water observed on the NW Iceland shelf in February is in the range of 27.74–27.8 kg/m³, continued winter cooling is likely to increase the density to be greater than 27.8 kg/m³ by the end of March (Figures 4e and 4f), and thus be able to contribute to the DSOW.

Figures 4a and 4b show the average February density profiles considering the years between 2000 and 2018 when the density on the shelf, in both sections, reached 27.74–27.8 kg/m³ (2001, 2005, 2007, 2009, 2010, and 2012 to 2015). Here, again top-to-bottom mixing in the inshore stations (on the shelf) can be observed even when the densities are below 27.8 kg/m³. However, if a heat loss equivalent to that shown by the model for

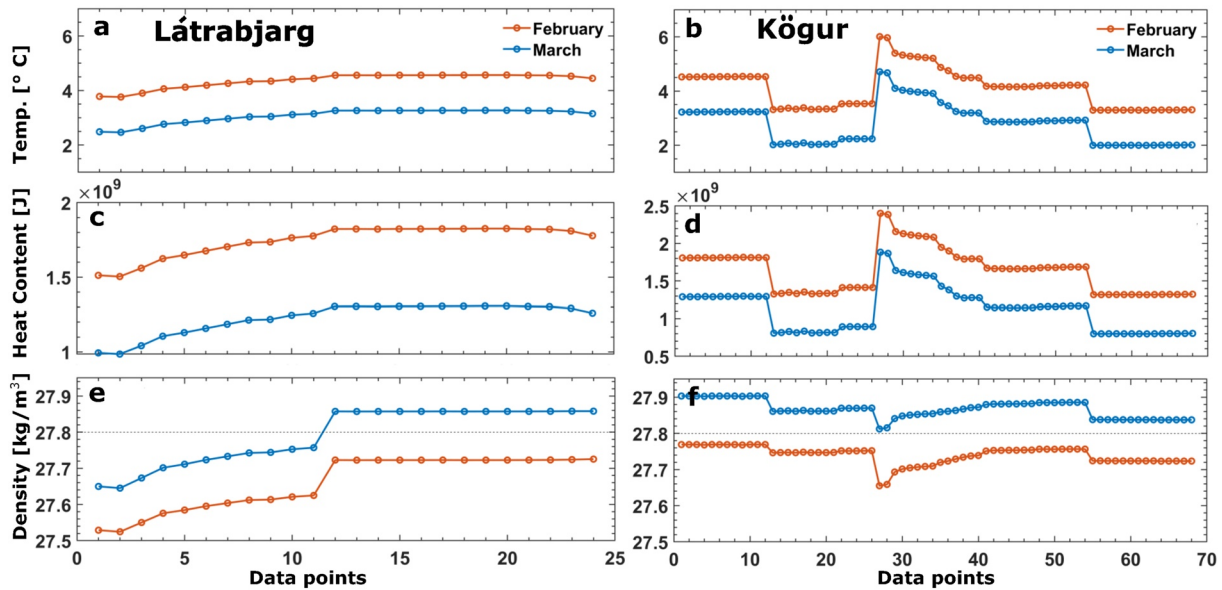


Figure 5. Observed February (orange) and 1D-mixing-model March (blue) temperature (a and b), heat content (c and d), and density (e and f) along the Látrabjarg (panels on the left) and the Kögur (panels on the right) sections. The sample data (temperature and salinity) points (x-axis) were selected from the years when the density on the shelf for both sections was lower than 27.8 kg/m^3 .

the month of March occurs (Figure 3c), we can see that the density along the shelf increases (Figures 4c and 4d), and just like in Figures 2a and 2b, appears to be distinct and well separated from the dense waters offshore.

Modeled March average density (Figures 4e and 4f) shows that densities larger than 27.8 kg/m^3 can still be found on the shelf during that month, indicating a persistent oceanic heat loss (Figure 3c). As such, with strong cooling even those years when the mean February density field does not show waters denser than 27.8 kg/m^3 on the shelf, they are likely to reach this density by the end of the winter. Thus, in most years it is likely that dense waters able to contribute to the DSOW could be formed on the Iceland shelf.

We then use the high-resolution numerical model configuration ANHA12 to explore the formation mechanisms and fate of the dense water once it is formed on the NW Icelandic shelf. Figure S1 suggests that the model is more saline on the Iceland shelf than the observations, which is reflected in the February density field, in particular near the base of the shelf (Figures S1a and S1b). However, even when the Atlantic inflow in the model is saltier (~ 0.25) than the observations this does not seem to have an impact on the deeper waters and the overflow, and thus the dynamics. As an example, Figures 6a–6c display a volume transport T-S diagram, which shows the mean volume transport (2002–2018) of the sections Kögur (Figure 6a), Húnaflói (Figure 6b), and Siglunes (Figure 6c), as a function of temperature and salinity (for each section its location is shown in the inset map in Figure 6). Consistent with Semper et al. (2019), see Figure 9 for reference, in the model the NIJ carries Arctic-origin water (temperature $< 0^\circ\text{C}$). Different from Semper et al. (2019), however, in the model the NIJ also carries dense (denser than 27.8 kg/m^3) waters with a temperature between 1 and 3°C and a salinity larger than 34.9. This water mass is potentially the dense water formed from the NIIC densification on the Icelandic shelf, which would explain its slightly larger salinity and higher temperature, compared to the denser waters carried by the main core of the NIJ.

Figures 6d–6f show the mean velocity (2002–2018) across the sections Kögur (Figure 6d), Húnaflói (Figure 6e), and Siglunes (Figure 6f). It shows that the model is properly simulating the positioning of the NIJ along the northern Icelandic shelfbreak and the magnitude of its velocity, consistent with Semper et al. (2019) (For comparison refer to Figure 4 in Semper et al., 2019). The overall agreement of the model with the observations means that we can examine the relevant dynamics in the model, consistent with the behavior in a high shelf density year, such as those listed above.

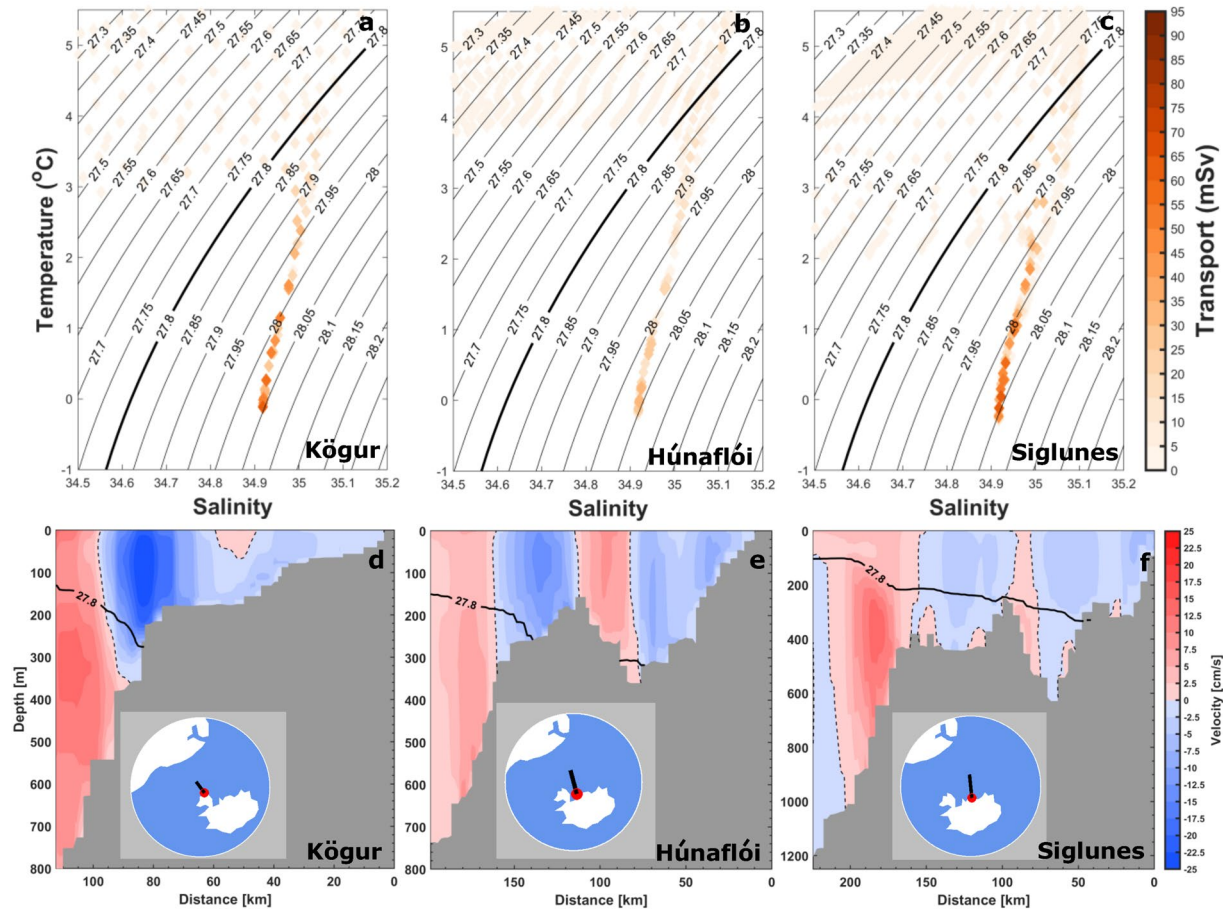


Figure 6. The upper panels show the mean (2002–2018) volume transport of the North Icelandic Jet as a function of temperature and salinity across the sections Kögur (a), Húnaflói (b), and Siglunes (c). For each section, the location is indicated in the inset map. In these diagrams, the thin black contours represent density. The lower panels show the mean (2002–2018) cross-section velocity for the sections Kögur (d), Húnaflói (e), and Siglunes (f). Positive velocities are directed toward Denmark Strait. In both cases (diagrams and sections), the upper limit of overflow water, defined by the 27.8 kg/m^3 , is highlighted by the thick black line. In the case of the sections (d–f), the zero velocity contour is marked by the dashed line.

4. Modeled Dense Water Formation on the NW Icelandic Shelf

In this section, we explore the processes involved in the formation of dense water on the western Icelandic shelf. To do so in detail, we use the year 2008 as a case study, to properly describe the formation of the dense plume, its evolution from the formation region, the large-scale circulation response and its potential contribution to the NIJ.

4.1. A Dense Plume Forms on the NW Icelandic Shelf

Once the dense water transformation on the shelf occurs, as discussed in the previous section, a dense plume (denser than 27.8 kg/m^3) travels eastward along the Icelandic shelf, cascading downslope at multiple locations. Such events occur almost every winter (January–March), except for the year 2003. Nonetheless we have chosen one particular episode, the winter of 2008 that shows the formation and subsequent path of the dense plume, so we can explain in detail the processes involved.

Figures 7a–7d show the evolution of a plume generated in January 2008. By the beginning of January, the transformed waters have already reached the bottom of the continental shelf (Figure 7a). By the end of January, the dense signature occupies a larger area and it has started to travel eastward along the shelf (Figure 7b). By February 24th the plume appears to start cascading down the shelf, north of Iceland (Figure 7c).

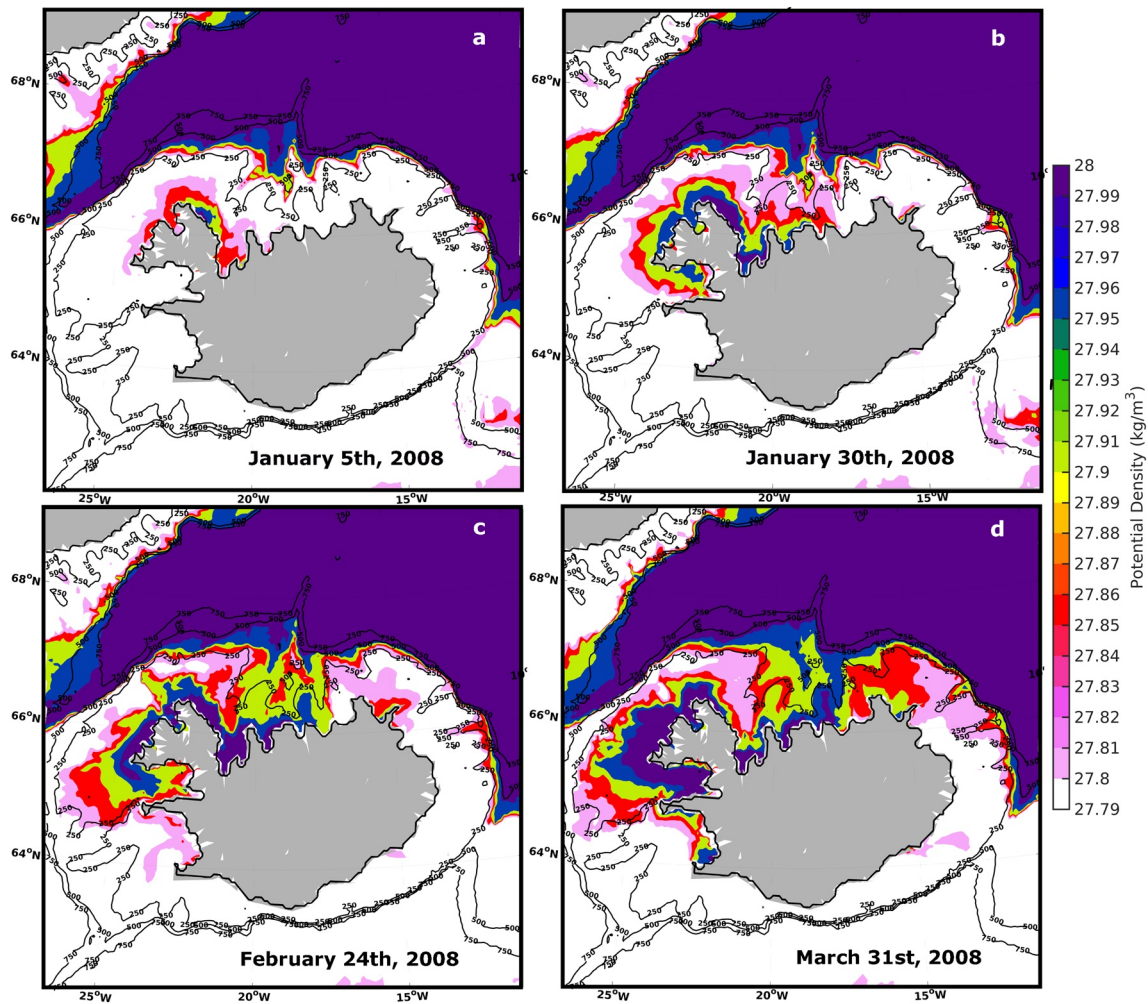


Figure 7. (a–d) Five-day average bottom density from four specific model outputs, from January 2008 to the end of March 2008. The exact date of each output is labeled on the bottom of each panel. Black contour lines indicate the 250, 500, and 750 m isobaths.

By March 31, the plume is connected with the already dense waters below 500 m depth in a more continuous pathway (Figure 7d), north of Iceland. Simultaneously, the initial dense signal located in the northwestern corner of the Icelandic shelf continues to grow in area.

4.2. Dense Waters Cascade Off the Shelf

To confirm the occurrence of a cascading event in the model we use Ivanov et al. (2004)'s density-dependent cascading parameter, r . Ivanov et al. (2004) states that “ r may be seen as a measure of descending potential of a cascade at any given cross slope section.” This parameter has previously been applied to explore dense water cascading in hydrostatic models (Luneva et al., 2020; Marson et al., 2017). Luneva et al. (2020) pointed out that “hydrostatic models are capable of reproducing the physics of cascading even on a steep slope.”

By strategically placing five points along a cross slope vertical section, Ivanov et al. (2004) defined a set of parameters that indicate the development stage of a cascading event. Here, however, we use only the density-dependent cascading parameter, r . According to Ivanov et al. (2004) the three relevant points (along a cross slope vertical section) that are needed to compute r , are: point A (e.g., Figure 8a) placed at the maximum density in the cascade (usually over the continental shelf); point B (e.g., Figure 8a) placed at the density minimum marking the position of the plume's edge; and point C (e.g., Figure 8a) located in the ambient water (undisturbed by the plume) at the same depth as A. As an example, Figure 8a shows the

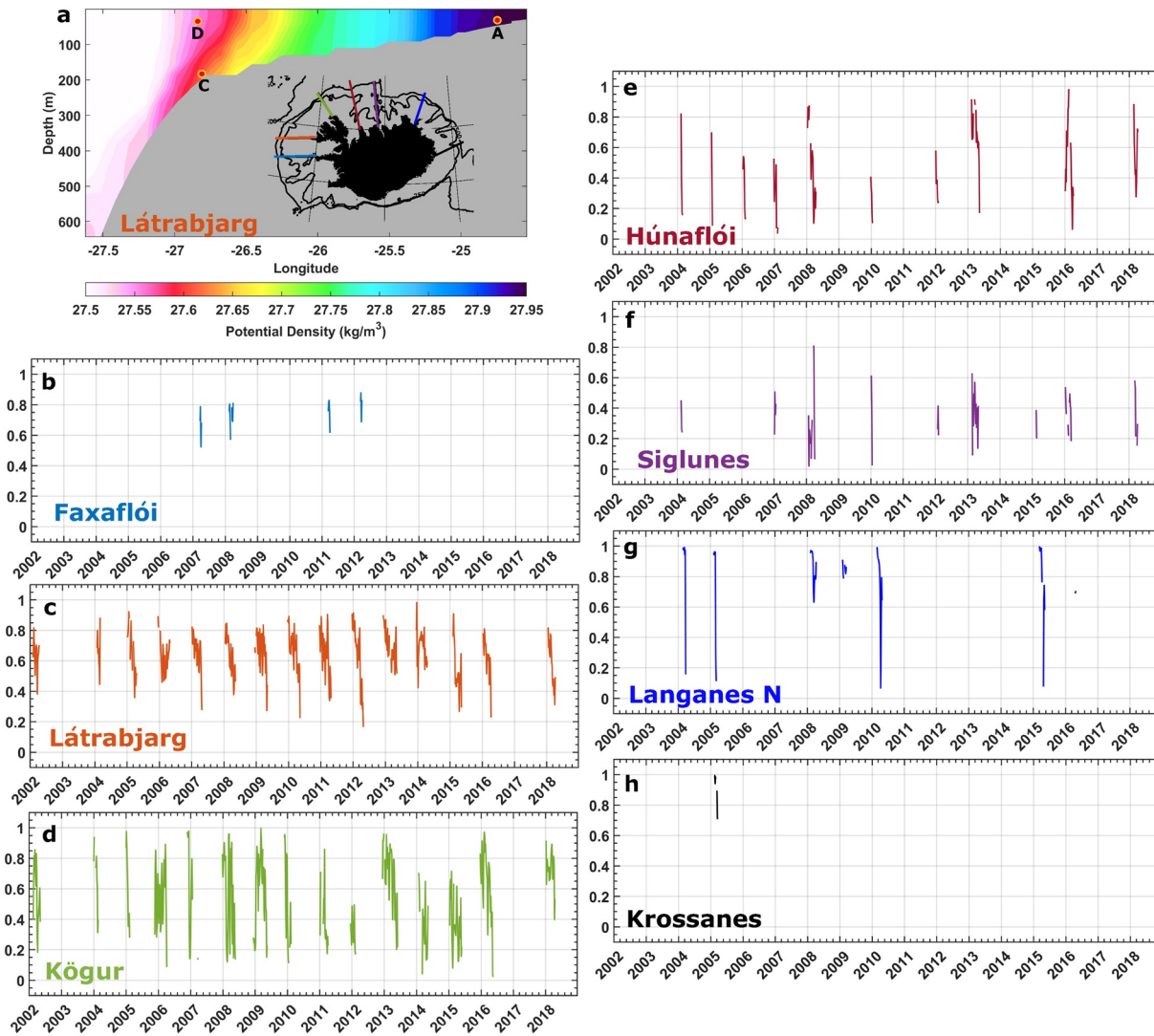


Figure 8. Cascading parameter r as a function of time, as defined by Ivanov et al. (2004), for the sections Faxaflói (b), Látrabjarg (c), Kögur (d), Húnaflói (e), Siglunes (f), Langanes N (g), and Krossanes (h). Panel a shows, by using the section Látrabjarg as an example, the position of the points A, B, and C needed to obtain the cascading parameter r . Colors of the section name on each panel, match the color of the sections shown on the inset map.

positioning of these points along the Látrabjarg section. Following this scheme, Ivanov et al. (2004) defined the cascading parameter, r , as:

$$r = \frac{\rho_A - \rho_B}{\rho_A - \rho_C} \quad (4)$$

where ρ_A is the density in point A, ρ_B is the density at point B, and ρ_C the density of the water at point C.

At the beginning of a cascading event r would be close to 1, since the density of the shelf waters (ρ_A) is significantly higher than both ambient (ρ_C) and shelfbreak waters (ρ_B). As the shelf waters progress down the slope, the density difference between the waters over the shelf and those at the bottom of the slope decreases ($\rho_A \approx \rho_B$), so r approaches zero.

Figures 8b–8h show time series of r , from 2002 to 2018, for most of the sections. As only values of r between zero and one are indicative of a cascading event occurrence, only values in that interval are shown. Thus, gaps in the time series indicate that no cascading event is registered along a given section. Except for Langanes E (not shown), cascading occurs along all the sections at least once during the study period (this is also confirmed in Video S3). It appears that once the dense water is formed on the west/northwest Icelandic

shelf, some of it cascades right away off the shelf (Figures 8b–8d), while the rest of the plume (as shown by the bottom density Video S1) travels eastward on the Icelandic shelf, cascading down slope along the north-shelf-located sections (Figures 8d–8h). This is consistent with Jungclauss and Backhaus (1994) who pointed out that in the long term a cascading event spreads from its source region mostly along isobaths and slightly downslope. This explains why we can see dense water cascading as far from the source region as along the Krossanes section. Note that Ivanov et al. (2004)'s parameter indicates when cascading occurs but not the amount of dense water formed on the shelf. As such, the potential contribution of dense waters formed on the shelf is explored in Section 4.4.

4.3. Large-Scale Circulation Response to the Dense Plume Formation and Propagation

Light waters are known to be linked to elevated SSH since low-density water expands and creates great steric height (Roughan et al., 2019). The contrary happens when the density of the water column increases as high-density water causes the SSH to decrease. The latter can be seen on the western Icelandic shelf. Dense water formation and the subsequent eastward propagation of the dense plume along the Icelandic shelf (Figure 7), results in the eastward propagation of low SSH from the region of dense water formation and along the topographic contours (Figures 9a–9d). In order to understand the evolution of the SSH due to the dense plume formation and the circulation response to it, we examined hourly model output, from October 2007 to May 2008.

As an example, Figure 9a, corresponding to March 20, 2008, at 00 h, shows a strong anti-cyclonic (eastward) circulation along the north Icelandic shelf. Within 24 h, an SSH depression develops on the western portion of the Icelandic shelf, and the flow previously anti-cyclonic (eastward) along the northern Icelandic shelf, changes to be cyclonic (westward) (Figure 9b). Thirteen hours later the SSH depression has continued traveling anti-cyclonically (eastward) while the flow direction appears strongly cyclonic (westward) along the north Icelandic shelf (Figure 9c). After another 24 h the SSH along the northern Icelandic shelf has risen (compared to Figure 9c) and the anti-cyclonic (eastward) flow has started to predominate (Figure 9d). Along the 500 m isobath, however, low SSH values remain (Figure 9d), which is most likely due to the dense water plume cascading down slope (Video S2). This particular event was triggered by the formation and evolution of the dense plume resulting from dense water formation in the winter of 2008 (Figure 7). The cyclonic (westward) flow described results from the propagation of the SSH signal. As the low SSH spreads eastward along the Icelandic shelf, it leaves behind a depression which is largest inshore and it decreases offshore. This results in a geostrophically balanced cyclonic (westward) flow along the north Icelandic shelf. This phenomenon was previously studied and proposed by Spall et al. (2017), who address the ocean response to localized dense water formation over closed topographic contours by applying a linear quasigeostrophic theory, a primitive equation model, and rotating-tank experiments.

Figures 9e–9g show cross section velocity for the Húnaflói section (inset map in Figure 9f) corresponding to March 16 (Figure 9e), 21 (Figure 9f), and 31 (Figure 9g), 2008. Note that the double-core structure of the NIJ is consistent with Pickart et al. (2017) and Semper et al. (2019). As the SSH intensifies and travels anti-cyclonically (eastward) on the shelf, the inner-core of the NIJ appears better defined and its velocity increases, while the outer-core's velocity decreases. This mismatch strengthening of the inner- and outer-cores was visible in most of our time series during the months of December (previous year) through May, coinciding with the months when the dense plume was found to form and the SSH depression to develop. Enhanced current velocities (like seen in Figure 9g) have been previously documented to be associated with dense shelf water formation in the Mediterranean Sea (Puig, 2017). Furthermore, this intensification of the NIJ inner-core could be linked to the identified (NIJ) regime during which the current is found to be strong and advecting anomalously dense water (Huang et al., 2019). This relationship, however, is not explored here.

4.4. Dense Water Cascading and Its Potential Contribution to the NIJ

Next, we examine the transport of waters denser than $27.8 \text{ kg} / \text{m}^3$ (upper limit of overflow water) carried by the plume along the shelf (clockwise), between the coast and the 250 m isobath. The transport is computed across the seven sections located around the northern Icelandic shelf (inset map in Figures 10a–10d). The

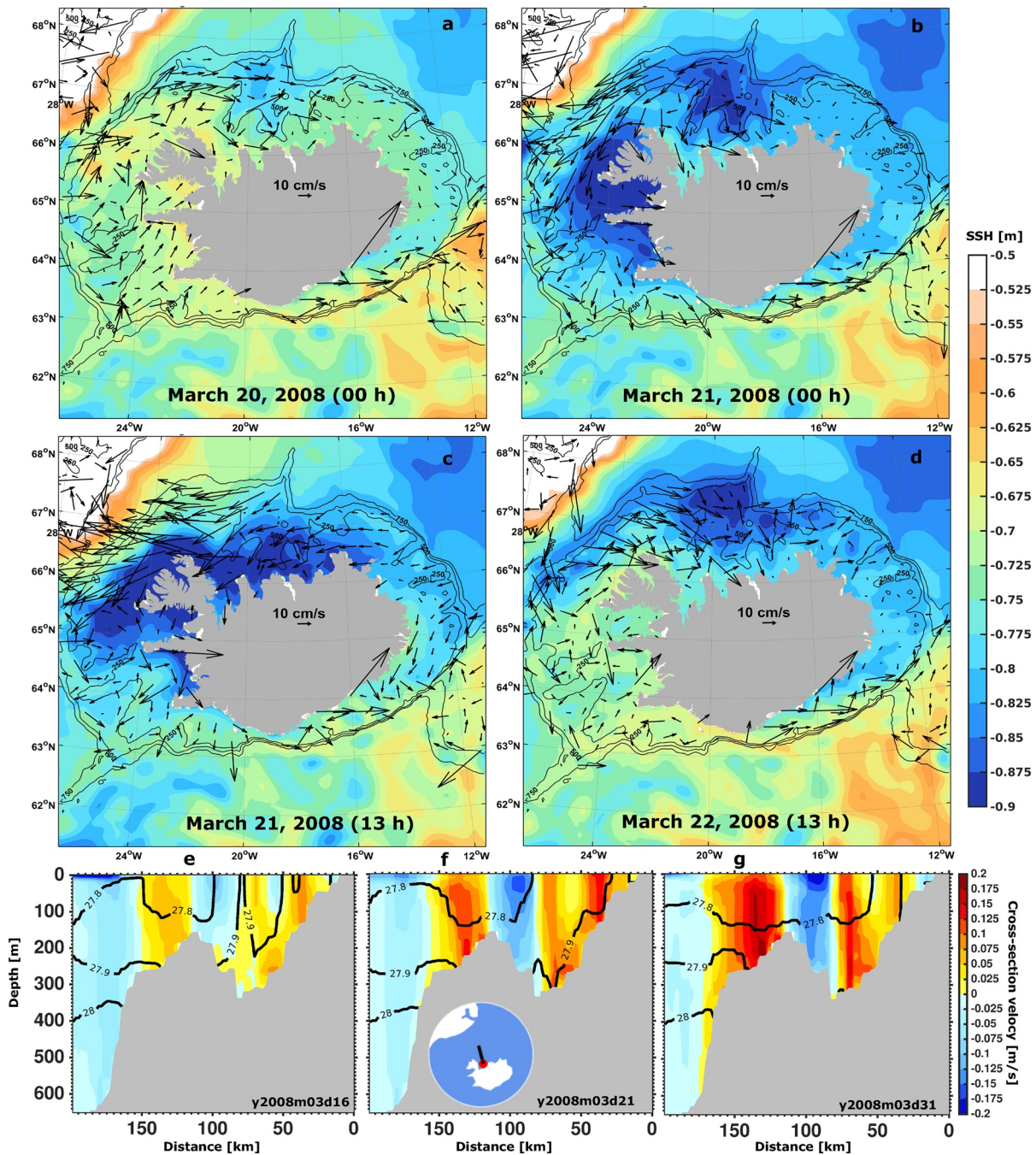


Figure 9. (a–d) Hourly mean sea surface height selected between March 20–22, 2008 (the exact time is labeled in each panel). The black arrows indicate the direction and magnitude of the flow at the surface. (e–g) Every-5-days mean vertical structure of the flow along the Húnaflói section (inset map), corresponding to March 16, 21, and 31, 2008. Positive values indicate eastward flow while negative velocity means westward flow.

selected sections are based on the hydrographic sections regularly monitored by the Marine and Freshwater Research Institute of Iceland.

Between the coast and the 250 m isobath, the direction of the along-isobath dense water flow is anti-cyclonic across all the sections (Figures 10a–10d). As the dense plume travels clockwise on the Icelandic shelf, its transport increases reaching a maximum of over 0.6 Sv along the Húnaflói section. This occurs during the months of February through April for the years 2002, 2004, 2005, 2008, 2013–2016, and 2018 (Figure 10b). For the years 2006 and 2009, it occurs during the months of December and May, respectively (Figure 10b).

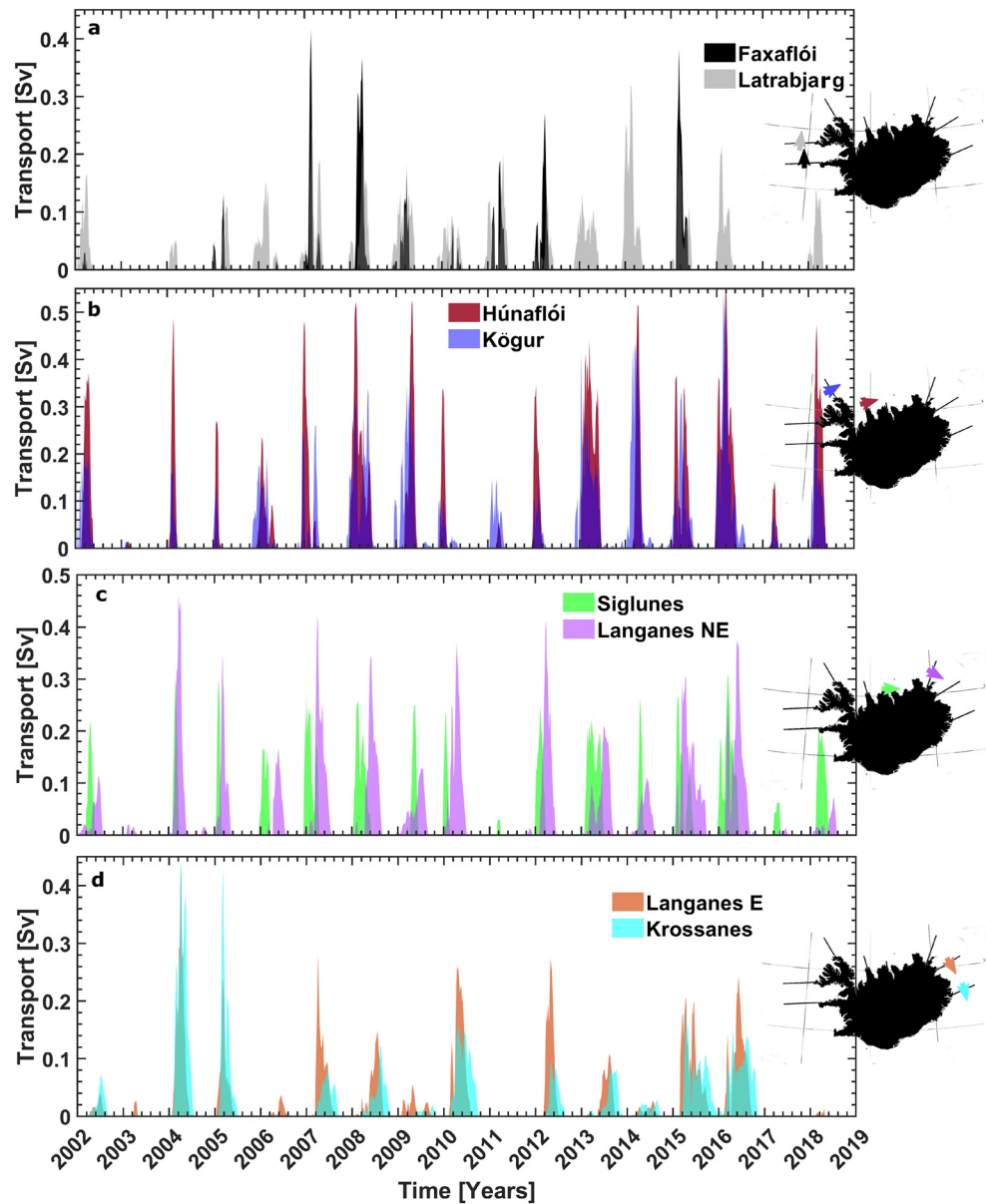


Figure 10. Time series of along-isobath transport of water denser than 27.8 kg/m^3 between the coast and 250 m depth, crossing the eight predetermined sections (inset map): Faxaflói (a), Látrabjarg (a), Kögur (b), Húnaflói (b), Siglunes (c), Langanes NE (c), Langanes E (d) and Krossanes (d).

The dense water transport across the next section (Siglunes), however, is lower, being above 0.5 Sv only during 2006 (December) and 2015 (February) (Figure 10c). This points out that the dense water cascades downslope at some point between the sections Húnaflói and Siglunes, most likely funneled through irregularities in the bathymetry along the northern Icelandic shelf (Figure 1). The dense water transport then increases slightly between the sections Langanes NE and Langanes E, but it mostly remains below 0.5 Sv, when at its maximum (Figure 10d). Here again there is evidence that a portion of the dense plume must have cascaded downslope between the Siglunes and the Langanes E sections.

To assess the magnitude of this downslope transport, we compute how much of the dense water plume cascades in between each section. Figure 11a shows that up to 0.1 Sv of dense water cascades in between the sections Faxaflói and Látrabjarg during the years 2005, 2007, 2008, 2010, 2011, 2012, and 2015 (positive values indicate cascading of waters denser than 27.8 kg/m^3). Considering its position, these cascading events

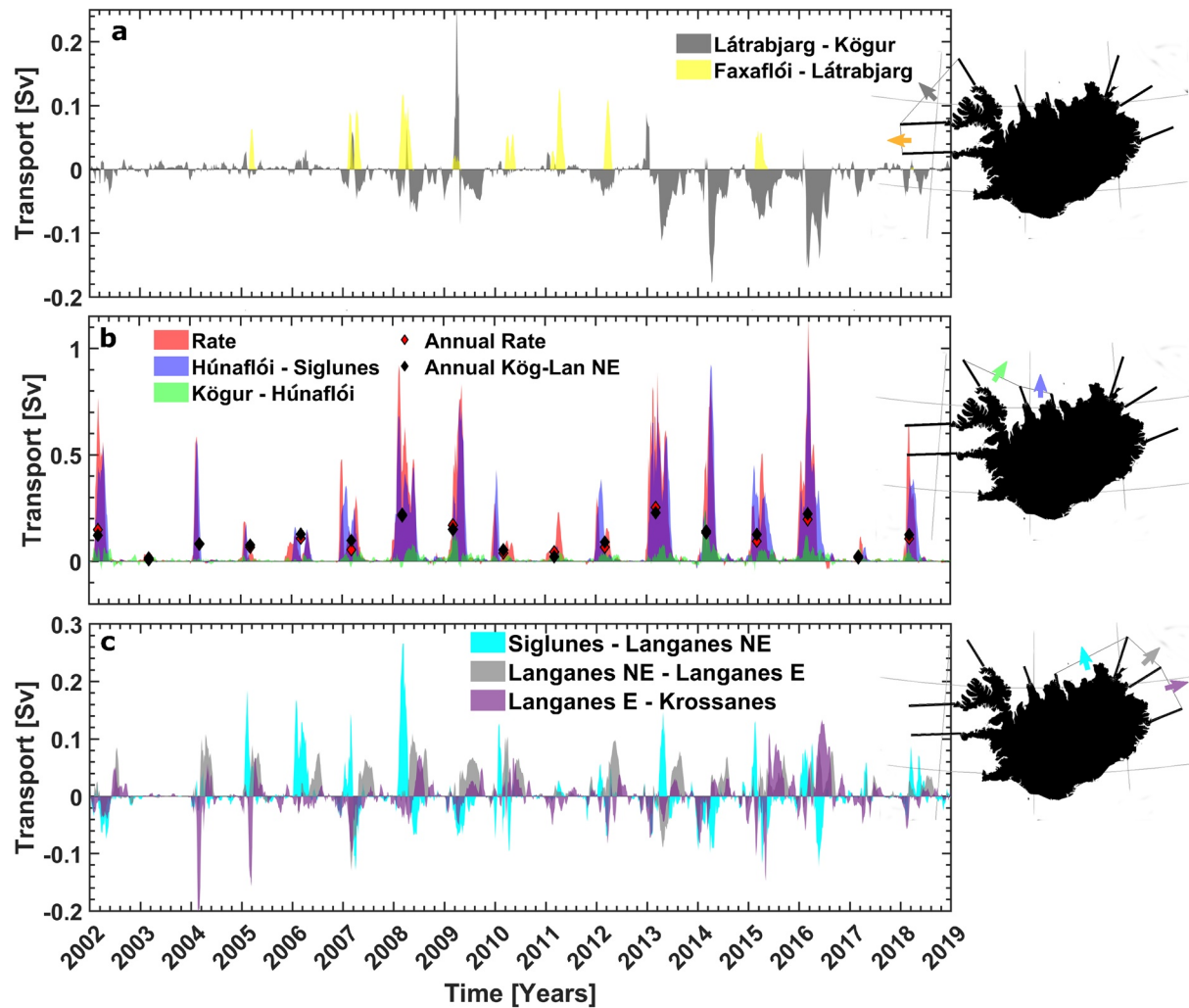


Figure 11. Time series of cross-isobath (250 m) transport of water denser than 27.8 kg/m^3 cascading down-slope (positive values) in between each consecutive section, from Faxaflói to Krossanes. The annual mean cross-isobath transport in between the Kögur and Langanes NE sections is shown (black diamonds in (c)). The every-5-days and annual means (red diamonds in (c)) cross-isobath (250 m) transport of waters denser than 27.8 kg/m^3 cascading down slope (positive values) from the formation region west of Iceland, referred to as Rate and Annual Rate respectively, are also shown.

potentially feed directly into the DSOW. Between the sections Látrabjarg and Kögur (Figure 11a) there is over 0.2 Sv of dense water cascading in 2009 and around 0.1 Sv in 2013, the rest of the years the (down-slope) dense water transport is very small. The cascading events occurred between the sections Kögur and Húnaflói (Figure 11b) in 2009, 2014, and 2016 resulted in around 0.1 Sv of dense water transported down-slope, being below that value for the rest of the years.

Figure 11b shows that the cross-isobath transport is the highest in between the sections Húnaflói and Siglunes. For comparison, we computed the overall dense water formed west of Iceland and it is shown as “Rate” (for dense water formation rate) in Figure 11b. It can be seen that, except for the year 2011, most of the dense water formed west of Iceland through shelf convection, cascaded downslope between the sections Húnaflói and Siglunes. During most years (2002, 2004, 2008, 2009, 2012, 2013, and 2015), these cascading events carried between 0.5 and 1 Sv of dense water off the Icelandic shelf. The annual mean for dense water formation rate (red diamonds) and for the cross-isobath transport of dense water between the sections Kögur and Langanes NE (black diamonds) are also shown in Figure 11b. The small difference in their magnitudes confirms that most of the dense water carried by the dense plume along the shelf, cascades north of Iceland.

Considering that the NIJ is centered near the 650 m isobath along the north Icelandic shelfbreak (Våge et al., 2011), we can assume that the dense water cascaded north of Iceland would ultimately join the current. In which case and as an example, the cascading events we found to occur in the winters of 2008, 2013, and 2016 between the sections Kögur and Langanes NE (black diamonds in Figure 11b), with an annual mean of 0.2 Sv of dense water cascaded down-slope, could have fed up to 21% of the NIJ transport at the Siglunes (Figure 6c) and Kögur sections (Figure 6a). These values are most likely underestimated considering they include periods when there is little or no cascading occurring.

4.4.1. Lagrangian Experiments

To support the dense water formation mechanism proposed here, we used the off-line Lagrangian tool known as Ariane (Blanke & Raynaud, 1997; Blanke et al., 1999) to track the upstream sources of the NIJ in the model. To do so, the particles were released along the Siglunes section and were set up to track waters denser than 27.8 kg / m^3 and with velocity to the west along the section. We selected the Siglunes section to release the particles for two main reasons: (a) most of the cascading in the model occurs in the region nearby this section (Figure 11), so we wanted for the particles to get “seeded” within the dense waters cascading from the shelf so we could backtrack the dense plume; and (b) the NIJ has not been merged with the EGC at the Siglunes section, so it was a way to make sure that we were only tracking dense waters carried by the NIJ. The actual number of particles initialized, n_i , around the i -th grid cell was determined based on:

$$n_i = N \left(\frac{V_i}{\sum_{j=1}^k V_j} \right) \left(\frac{v_i}{\bar{v}} \right), i \in 1..k, \quad (5)$$

where k is the number of grid points which meet the criteria, v_i is the velocity of each identified grid cell, \bar{v} is the mean velocity of each identified grid cell, V_i is the volume of each identified grid cell, V_j is the total volume of identified grid cells, and N is the total number of particles to be initialized. The initial position of the particles at the beginning of each experiment is shown in Figure S6. The particles were tracked backward in time from 2019 to 2004, with around 10,000 particles (N) released every month of 2019, for a total of 12 experiments. The experiments were started in 2019 to be able to integrate the particles for 15 years while avoiding the initial spin-up years.

Figure 12 shows the 1-year evolution for the particles released at the beginning of every month, from January to April, 2019. During these months (January–April), the heat loss west of Iceland is the strongest (Figure 3) and the selected experiments capture the consequent transformation of the seeded particles. Also, we consider 1-year tracking to be enough to explore this particular process. The Lagrangian particles (Figure 12) show that there are two different pathways that feed into the NIJ in the Siglunes section: dense waters of Arctic-origin reaching the section with densities already higher than 27.95 kg / m^3 and whose pathway coincides with that proposed by De Jong et al. (2018); and dense waters from the western Icelandic shelf that result from the transformation of the NIIC as it travels on the western Icelandic shelf. This supports the presence of Arctic-origin water and a warmer and saltier dense water found to contribute to the NIJ along the Siglunes section shown in the volume transport T-S diagram (Figure 6c). As suggested before, the Atlantic inflow transformation is more prominent during the months of March (Figures 12g–12i) and April (Figures 12j–12l), which coincides with the months when the oceanic heat loss is the strongest. The transformation occurs on the western Icelandic shelf, within water depths of 250 m, supporting our theory of shelf convection occurrence in the region.

5. Discussion and Conclusions

In this paper, we investigated the transformation of the NIIC through shelf convection NW of Iceland and its link to the NIJ, using observational data and numerical model simulation results. Analysis of the observational data shows that overflow waters are present on the western Icelandic shelf, appearing well mixed in the water column. The density of these waters can potentially increase as the winter progresses and oceanic heat loss continues. We then make use of numerical output to investigate the origin and fate of these waters. By using $1 / 12^\circ$ horizontal resolution model output (2002–2018), we investigated the transformation of the inflowing NIIC on the west/northwest portion of the Icelandic shelfbreak (as the source of the dense waters found on the shelf in the observations) and the potential contribution of the transformed waters to the NIJ.

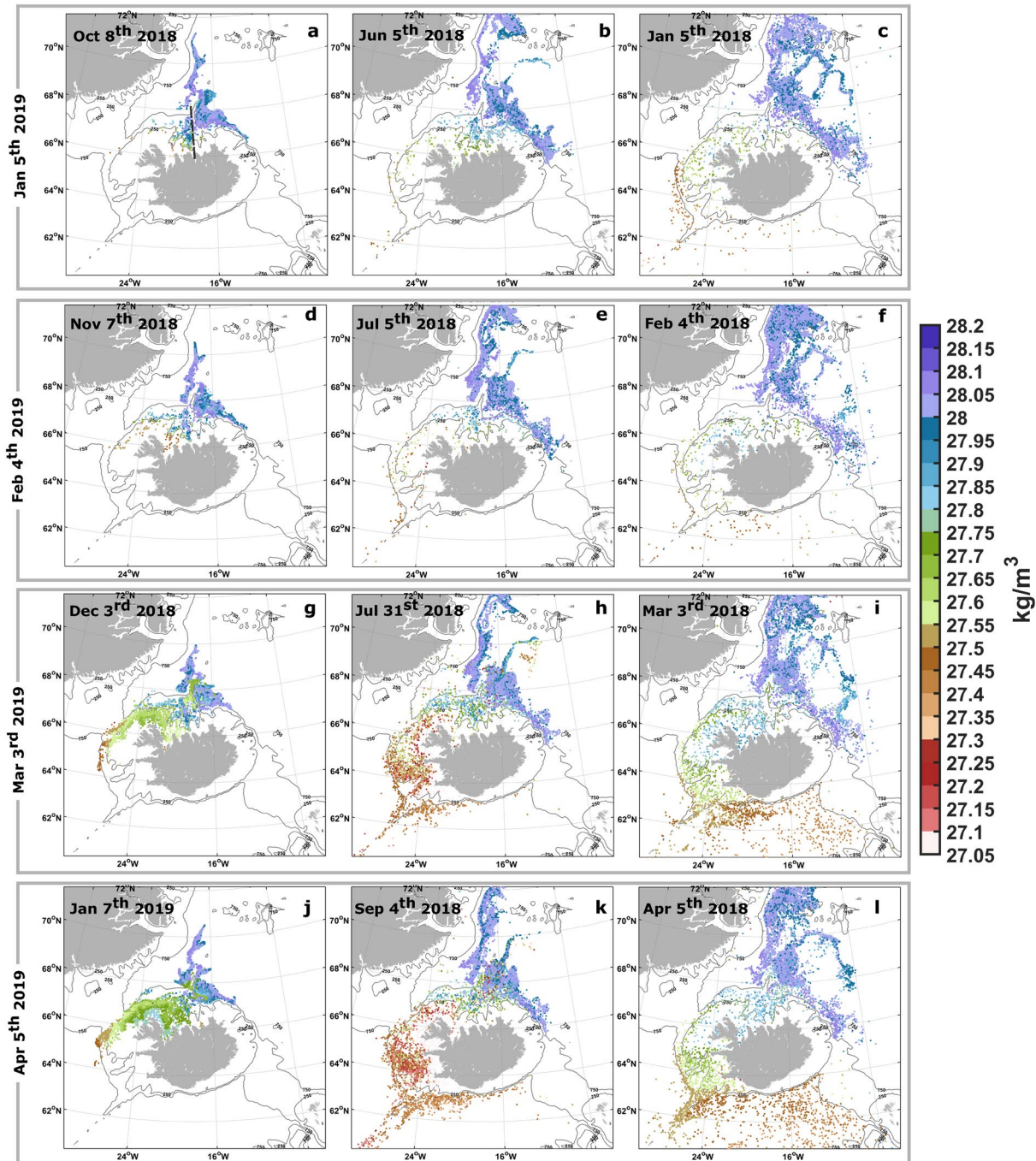


Figure 12. One-year density evolution for particles released monthly along the Siglunes section, from January to April of 2019, backtracking the upstream sources of the North Icelandic Jet. Panels (a–c) show the evolution of the particles released in January 5. Panels (d–f) show the evolution of the particles released in February 4. Panels (g–i) show the evolution of the particles released in March 3. Panels (j–l) show the evolution of the particles released in April 5. The released date can be seen at the left of the panels (a) (January), (d) (February), (g) (March), and (j) (April). The date found in the upper-left corner of each panel corresponds to the time of the model output for each case. The color indicates the density of the particles at that specific place and time (upper-left corner of each panel). The dashed black line in panel (a), corresponds to the position of the Siglunes section where the particles were released.

As a summary of our findings, we propose the following circulation scheme (Figure 13): as the NIIC travels around the Westfjords, strong winter heat loss allows the surface waters to gain in density and sink down to the bottom. This dense water formation process generates a dense plume that travels anti-cyclonically on the shelf, with some waters cascading off the shelf near the formation region west of Iceland (up to

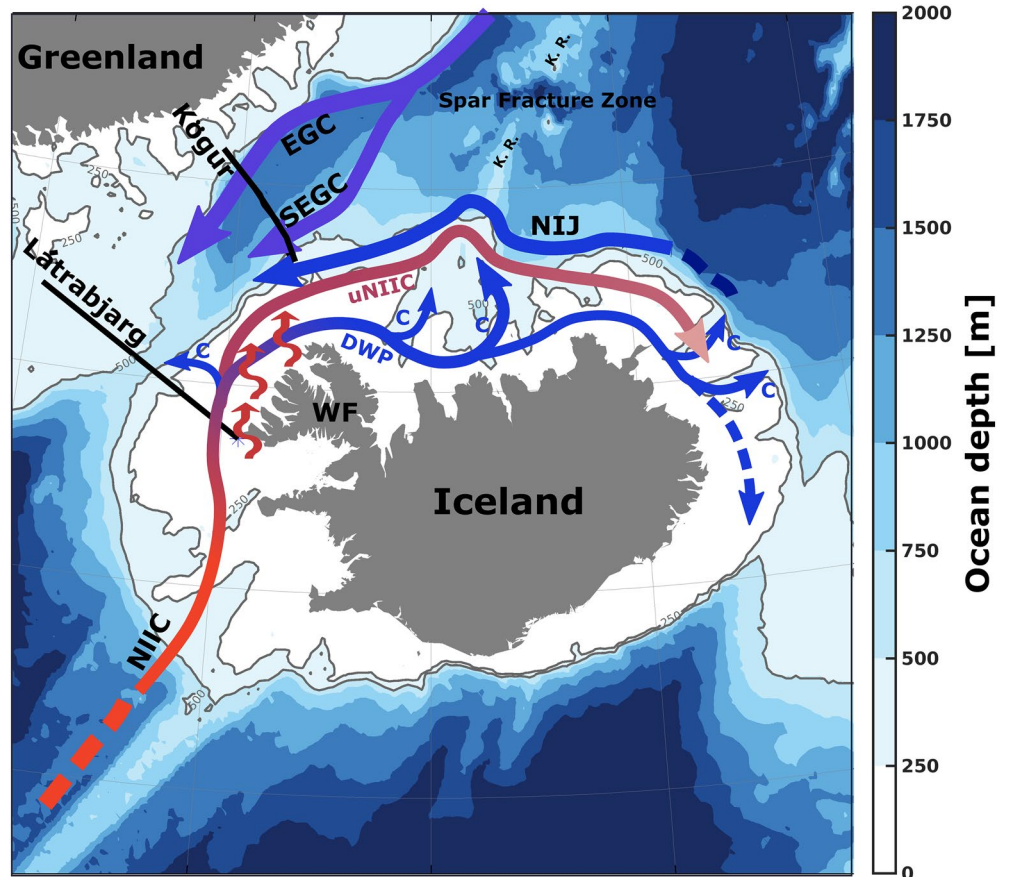


Figure 13. Updated schematic circulation in the vicinities of Iceland adding the mechanism proposed in the manuscript. The main currents shown and their acronyms are: shelfbreak East Greenland Current (EGC), separated East Greenland Current (SEGC), North Icelandic Irminger Current (NIIC), and the North Icelandic Jet (NIJ). The region northwest of Iceland known as the Wester Fjords is identified as WF. The Kolbeinsey Ridge is represented as K. R. in the map. The wiggly red lines around the Wester Fjords region represents the winter heat loss, pointing out that this is the region where shelf convection occurs. The pathway followed by the dense water plume (DWP) once is formed along the Icelandic shelf is represented by the blue arrow line closer to the northern Icelandic coast. The acronym uNIIC (“u” for untransformed) corresponds to the NIIC waters that are not density and follow their known pathway north of Iceland. The cascading locations found (labeled with the letter C in the map) are represented by the short arrow lines that separates from the DWP.

0.2 Sv in some years; Figure 11a), but with the bulk of the water cascading off the shelf north of Iceland. In both cases, deep cross-shelf troughs along Icelandic shelf seem to act as channels for the dense waters to flow downslope. The dense waters that cascade along the northern section travel cyclonically along the Icelandic shelfbreak within the (cyclonic) flow resultant from the SSH gradient. The overall result is an enhanced equatorward flow on the continental slope, which is consistent with the strong NIJ regime (Huang et al., 2019). In years of strong cascading events the dense plume was found to contribute, on an annual average, up to 21% of the NIJ transport.

The dense waters cascaded off the shelf west of Iceland would contribute directly to the DSOW, as previously suggested by the literature (Saber et al., 2020). While using Lagrangian backtracking of the DSOW sources in a realistic numerical ocean simulation, Saber et al. (2020) found additional pathways from south of Iceland. They state that the largest contribution from these pathways to the DSOW (25.8% during the winter of 2008) is seen when there is more dense water on the Icelandic shelf. This is also in line with our findings as the densification of the NIIC occurs when the heat loss is the strongest (winter months January–March), hence more dense water (denser than 27.8 kg / m^3) is found on the Icelandic shelf.

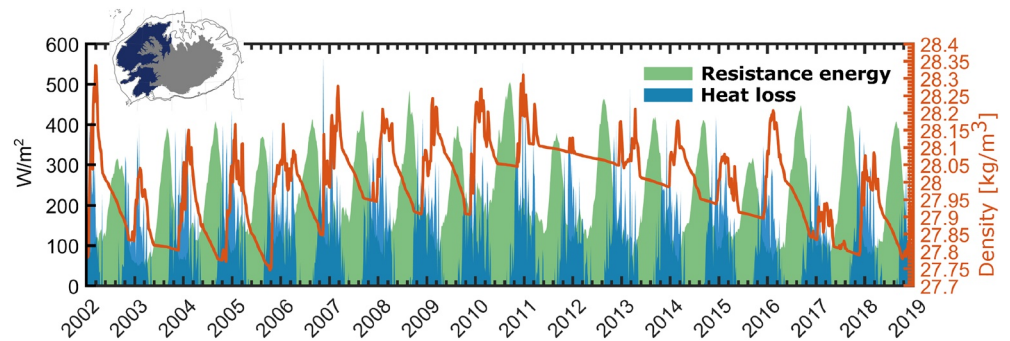


Figure 14. Time series of heat loss, maximum density and resistance energy as a function of the time on the western Icelandic shelf (blue colored region—inset map).

A physical explanation for the dense plume evolution and the large-scale circulation response to it, is provided by Spall et al. (2017). By using a primitive equation model and rotating-tank experiments, they investigated the circulation response to a localized dense water formation region over a sloping bottom. Their work was motivated by “topography around islands or shallow shoals in which convection resulting from brine rejection or surface heat loss reaches the bottom” (Spall et al., 2017). Just like we showed here (Figure 9), they found that a SSH depression propagates from the formation region anticyclonically, around the island. As a response, a cyclonic current is generated around the topography, traveling in the opposite way of the dense water plume at a speed in the range of 2–15 cm/s. There are, however, some differences between our findings and Spall et al. (2017)s: (a) in our case, the cascading points are linked to irregularities in the bathymetry; and (b) the resultant cyclonic flow is only seen along the northern Icelandic slope and not all around the island as in Spall et al. (2017). That being said their idealized model and tank experiments consider the bathymetry around the island to be smooth. As such, submarine canyons or features like the Denmark Strait sill are not represented in their study.

Our results are also in agreement with Huang et al. (2019) who found that larger heat fluxes over the study region lead to an enhanced signature of the NIJ 2 months later along the Kögur section. In fact, enhanced current velocities associated to dense shelf waters cascading have been documented (Puig, 2017). Considering our findings, from a cascading point in the vicinities of the Siglunes section (Figure 7c), at a speed of 15 cm/s (Figure 9f), it would take the dense waters ~20 days to reach the Kögur section. This is, similar to Huang et al. (2019), ~2 months after the heat loss is at its maximum around the formation region.

The observed formation of dense waters on the Icelandic shelf, however, does not appear to occur every February. The observations show shelf convection occurring in the month of February on the NW Icelandic shelf, with dense waters reaching over 27.8 kg / m^3 during the years 1983, 1984, 1988, 1997, 2004, 2011, and 2016 (Figures 2a and 2b and Figure S5). However, based on a simple 1-D mixing model we showed that in other years when lower densities are observed during the month of February, continued heat loss during the month of March is likely to increase the density to the range associated with the lightest component of the DSOW.

Model data indicate that the winter heat loss west of Iceland is enough to densify the waters carried by the NIIC. Figure 14 compares heat loss, resistant energy (RE) and maximum density west of Iceland (dark blue region inset map—Figure 14). RE is defined as the amount of energy needed to be removed from a given region, such that the density will become homogenized down to a certain depth (Holdsworth & Myers, 2015). The mathematical expression to compute the resistance energy is expressed as:

$$RE(h) = \frac{g}{A} \iint \left[h \rho_{pot}(h) - \int_0^h \rho_{pot}(z) dz \right] dA \quad (6)$$

where g is the gravitational constant, A is the surface area of each grid cell, $\rho_{pot}(z)$ and $\rho_{pot}(h)$ are the potential density at each grid cell and the potential density of the grid cell at the reference depth h , respectively. In our case of study $h = 250 \text{ m}$.

Figure 14 shows that when the density reaches its maximum, the heat loss exceeds the resistance energy. This means that, the amount of energy removed from the ocean due to heat loss is indeed enough to increase the density of the surface waters, making them sink while homogenizing the entire water column. Note that the maximum winter heat loss is over 200 W/m^2 every year (2002–2018), going over the 300 W/m^2 for some years. This shows that the mean heat loss magnitude removed from the observations in February (analysis shown in Section 3) is not only sufficient but also an underestimation in some years, in which case the heat loss could be stronger and the density of the waters formed on the shelf larger. During some years, however, even when waters denser than 27.8 kg/m^3 are found in the formation region (Figure 6) and the maximum winter heat loss exceeds the 300 W/m^2 , no dense plume is generated. This is the case of the year 2003 (Figure 11b, Video S1). This means that a strong winter heat loss will not necessarily trigger the dense plume formation mechanism and that other factors could be at play, which needs further study.

Nonetheless, our results point out that given the relation between the oceanic heat loss and shelf convection, the recurrence of the latter is likely to depend on a specific atmospheric pattern, most likely coinciding with Saberi et al. (2020), the NAO. Unfortunately, hydrographic data after the year 2000 for the months of March and April which is when the model shows the strongest transformation to occur (Figures 12g–12l), is scarce. In fact, the database used here only had data collected in the month of March for the year 2004 and along the Faxaflói section, which is south from the formation region and as such it did not capture the shelf convection event that year.

As the modeled NIIC inflow is somewhat saltier compared to the observations (~ 0.25), the formation of the dense plume might be interpreted as an artificial signal of the model induced by a salinity bias. However, the volume transport T-S diagram constructed for the sections Kögur, Húnaflói, and Siglunes (Figures 6a–6c) shows that this does not seem to impact the transport and properties of the dense waters carried by the NIJ, and thus the dynamics. We are able to see the formation of the dense plume right from the beginning of the simulation, when the model is started from a reanalysis product that assimilates observed temperature and salinity data (Ferry et al., 2016). We were also able to find the presence of the dense plume and the consequent response of the SSH (Figure S4) in the model reanalysis product Global Ocean 1/12° Physics Analysis and Forecast (GLOBAL ANALYSIS FORECAST PHY-001-024), traditionally referred to as PSY4 (Supporting Information S1). In any case, we are using the model to understand the large-scale processes, so understanding the specific details may need to be further refined.

To further understand the mechanisms proposed here and in what way they could be potentially impacted by ongoing climate change, they need to be explored with in situ observations, specifically during the month of March and April. Even if the waters formed through the mechanism proposed here contribute to the lighter component of the NIJ, these findings are of a great significance given that the Icelandic shelf as a source of the NIJ has not been proposed before. What is more, the occurrence of shelf convection west of Iceland means that ocean ventilation, which is known to occur only in a few regions of the world's ocean, could be taking place.

References

- Barnier, B., Madec, G., Penduff, T., Molines, J.-M., Treguier, A.-M., Sommer, J. L., et al. (2006). Impact of partial steps and momentum advection schemes in a global ocean circulation model at eddy-permitting resolution. *Ocean Dynamics*, 56(5–6), 543–567. <https://doi.org/10.1007/s10236-006-0082-1>
- Behrens, E., Våge, K., Harden, B., Biastoch, A., & Böning, C. W. (2017). Composition and variability of the Denmark Strait Overflow Water in a high-resolution numerical model hindcast simulation. *Journal of Geophysical Research: Oceans*, 122(4), 2830–2846. <https://doi.org/10.1002/2016JC012158>
- Blanke, B., Arhan, M., Madec, G., & Roche, S. (1999). Warm water paths in the Equatorial Atlantic as diagnosed with a General Circulation Model. *Journal of Physical Oceanography*, 29(11), 2753–2768. [https://doi.org/10.1175/1520-0485\(1999\)029<2753:wwpite>2.0.co;2](https://doi.org/10.1175/1520-0485(1999)029<2753:wwpite>2.0.co;2)
- Blanke, B., & Raynaud, S. (1997). Kinematics of the Pacific Equatorial Undercurrent: An Eulerian and Lagrangian approach from GCM results. *Journal of Physical Oceanography*, 27(6), 1038–1053. [https://doi.org/10.1175/1520-0485\(1997\)027<1038:kotpeu>2.0.co;2](https://doi.org/10.1175/1520-0485(1997)027<1038:kotpeu>2.0.co;2)
- Canals, M., Danovaro, R., Heussner, S., Lykousis, V., Puig, P., Trincardi, F., et al. (2009). Cascades in Mediterranean submarine grand canyons. *Oceanography*, 22(1), 26–43. <https://doi.org/10.5670/oceanog.2009.03>
- Canals, M., Puig, P., de Madron, X. D., Heussner, S., Palanques, A., & Fabres, J. (2006). Flushing submarine canyons. *Nature*, 444, 354–357. <https://doi.org/10.1038/nature05271>
- Chapman, D. C., & Gawarkiewicz, G. (1995). Offshore transport of dense shelf water in the presence of a submarine canyon. *Journal of Geophysical Research*, 100(C7), 13373–13387. <https://doi.org/10.1029/95JC00890>

Acknowledgments

The authors gratefully acknowledge the financial and logistic support of grants from the Natural Sciences and Engineering Research Council (NSERC) of Canada. These include a Discovery Grant (rgpin227438-09) awarded to P. G. Myers, Climate Change and Atmospheric Research Grant (VITALS-RG-PCC 433898), and an International CREAT (ArcTrain-432295). The authors are grateful to the NEMO development team and the Drakkar project for providing the model and continuous guidance. The authors would also like to thank G. Smith for the CGRF forcing fields, made available by Environment and Climate Change Canada (http://weather.gc.ca/grib/grib2_glb_25km_e.html). The authors gratefully acknowledge the Kögur Project whose data were used for model evaluation and is freely available on <http://kogur.whoj.edu/>. The authors are thankful for the International Council for the Exploration of the Sea (ICES) database (<https://ices.dk/marine-data/dataset-collections/>), used here to explore the presence of dense water on the continental Icelandic shelf. The authors are grateful for the Physics Analysis and Forecast (GLOBAL ANALYSIS FORECAST PHY-001-024, traditionally referred to as PSY4) data, available on Copernicus Marine Environmental Monitoring Service (<http://marine.copernicus.eu/>). The authors thank Westgrid and Compute Canada for computational resources, where all model experiments were performed and are archived (<http://www.computecanada.ca/>). The authors also thank two anonymous reviewers for suggesting substantial improvements to the manuscript.

- Clark, C. D., & Spagnolo, M. (2016). Glacially eroded cross-shelf troughs surrounding Iceland from Olex data. *Geological Society, London, Memoirs*, 46(1), 165–166. <https://doi.org/10.1144/M46.86>
- De Jong, M. F., Soiland, H., Bower, A., & Furey, H. (2018). The subsurface circulation of the Iceland Sea observed with RAFOS floats. *Deep Sea Research Part I: Oceanographic Research Papers*, 07, 1–10. <https://doi.org/10.1016/j.dsr.2018.07.008>
- Ferry, N., Parent, L., Masina, S., Storto, A., Zuo, H., & Balmaseda, M. (2016). *Product user manual for Global Ocean Reanalysis Products GLOBAL-REANALYSIS-PHYS-001-009, GLOBAL-REANALYSIS-PHYS-001-011 and GLOBAL-REANALYSIS-PHYS-001-017 (Computer software manual No. 2.9)*.
- Fichefet, T., & Maqueda, M. (1997). Sensitivity of a global sea ice model to the treatment of ice thermodynamics and dynamics. *Journal of Geophysical Research*, 102(C6), 12609–12646. <https://doi.org/10.1029/97JC00480>
- Grivault, N., Hu, X., & Myers, P. G. (2018). Impact of the surface stress on the volume and freshwater transport through the Canadian Arctic Archipelago from a high-resolution numerical simulation. *Journal of Geophysical Research: Oceans*, 123(12), 9038–9060. <https://doi.org/10.1029/2018JC013984>
- Harden, B., Pickart, R., Valdimarsson, H., Våge, K., de Steur, L., Richards, C., et al. (2016). Upstream sources of the Denmark Strait Overflow: Observations from a high-resolution mooring array. *Deep Sea Research Part I: Oceanographic Research Papers*, 112, 94–112. <https://doi.org/10.1016/j.dsr.2016.02.007>
- Holdsworth, A. M., & Myers, P. G. (2015). The influence of high-frequency atmospheric forcing on the circulation and deep convection of the Labrador Sea. *Journal of Climate*, 28(12), 4980–4996. <https://doi.org/10.1175/JCLI-D-14-00564.1>
- Hu, X., Myers, P. G., & Lu, Y. (2019). Pacific water pathway in the Arctic Ocean and Beaufort Gyre in two simulations with different horizontal resolutions. *Journal of Geophysical Research: Oceans*, 124(8), 6414–6432. <https://doi.org/10.1029/2019JC015111>
- Hu, X., Sun, J., Chan, T. O., & Myers, P. G. (2018). Thermodynamic and dynamic ice thickness contributions in the Canadian Arctic Archipelago in NEMO-LIM2 numerical simulations. *The Cryosphere*, 12(4), 1233–1247. <https://doi.org/10.5194/tc-12-1233-2018>
- Huang, J., Pickart, R. S., Valdimarsson, H., Lin, P., Spall, M. A., & Xu, F. (2019). Structure and variability of the North Icelandic Jet from two years of mooring data. *Journal of Geophysical Research: Oceans*, 124, 3987–4002. <https://doi.org/10.1029/2019JC015134>
- Ivanov, V., & Golovin, P. N. (2007). Observations and modeling of dense water cascading from the Northwestern Laptev Sea shelf. *Journal of Geophysical Research*, 112(C9). <https://doi.org/10.1029/2006JC003882>
- Ivanov, V., Maslov, P., Aksenov, Y., & Coward, A. (2015). Shelf-basin exchange in the Laptev Sea in the warming climate: A model study. *Geophysical & Astrophysical Fluid Dynamics*, 109, 254–280. <https://doi.org/10.1080/03091929.2015.1025776>
- Ivanov, V., Shapiro, G., Huthnance, J., Aleynik, D., & Golovin, P. (2004). Cascades of dense water around the world ocean. *Progress in Oceanography*, 60(1), 47–98. <https://doi.org/10.1016/j.pocean.2003.12.002>
- Jochumsen, K., Köllner, M., Quadfasel, D., Dye, S., Rudels, B., & Valdimarsson, H. (2015). On the origin and propagation of Denmark Strait overflow water anomalies in the Irminger Basin. *Journal of Geophysical Research: Oceans*, 120(3), 1841–1855. <https://doi.org/10.1002/2014jc010397>
- Jochumsen, K., Moritz, M., Nunes, N., Quadfasel, D., Larsen, K. M. H., Hansen, B., et al. (2017). Revised transport estimates of the Denmark Strait overflow. *Journal of Geophysical Research: Oceans*, 122(4), 3434–3450. <https://doi.org/10.1002/2017JC012803>
- Jonsson, S., & Valdimarsson, H. (2004). A new path for the Denmark Strait overflow water from the Iceland Sea to Denmark Strait. *Geophysical Research Letters*, 31. <https://doi.org/10.1029/2003GL019214>
- Jungclauss, J. H., & Backhaus, J. O. (1994). Application of a transient reduced gravity plume model to the Denmark Strait overflow. *Journal of Geophysical Research*, 99(C6), 12375–12396. <https://doi.org/10.1029/94jc00528>
- Kämpf, J. (2005). Cascading-driven upwelling in submarine canyons at high latitudes. *Journal of Geophysical Research*, 110(C2). <https://doi.org/10.1029/2004JC002554>
- Käse, R. H., Serra, N., Köhl, A., & Stammer, D. (2009). Mechanisms for the variability of dense water pathways in the Nordic Seas. *Journal of Geophysical Research*, 114(C1). <https://doi.org/10.1029/2008JC004916>
- Killworth, P. D. (1983). Deep convection in the world ocean. *Reviews of Geophysics*, 21(1), 1–26. <https://doi.org/10.1029/RG021i001p00001>
- Köhl, A. (2010). Variable source regions of Denmark Strait and Faroe Bank Channel overflow waters. *Tellus A*, 62(4), 551–568. <https://doi.org/10.1111/j.1600-0870.2010.00454.x>
- Köhl, A., Käse, R. H., Stammer, D., & Serra, N. (2007). Causes of changes in the Denmark Strait overflow. *Journal of Physical Oceanography*, 37(6), 1678–1696. <https://doi.org/10.1175/JPO3080.1>
- Large, W. G., & Yeager, S. G. (2004). *Diurnal to decadal global forcing for ocean and sea-ice models: The data sets and flux climatologies (NCAR Technical Note)*.
- Large, W. G., & Yeager, S. G. (2009). The global climatology of an interannually varying air–sea flux data set. *Climate Dynamics*, 33(2), 341–364. <https://doi.org/10.1007/s00382-008-0441-3>
- Luneva, M. V., Ivanov, V. V., Tuzov, F., Aksenov, Y., Harle, J. D., Kelly, S., & Holt, J. T. (2020). Hotspots of dense water cascading in the Arctic Ocean: Implications for the Pacific water pathways. *Journal of Geophysical Research: Oceans*, 125(10), e2020JC016044. <https://doi.org/10.1029/2020JC016044>
- Madec, G., & the NEMO team. (2008). *Nemo ocean engine (Note du Pôle de modélisation)*. Institut Pierre-Simon Laplace (IPSL).
- Magaldi, M. G., & Haine, T. W. (2015). Hydrostatic and non-hydrostatic simulations of dense waters cascading off a shelf: The east Greenland case. *Deep Sea Research Part I: Oceanographic Research Papers*, 96, 89–104. <https://doi.org/10.1016/j.dsr.2014.10.008>
- Marson, J. M., Myers, P. G., Hu, X., Petrie, B., Azetsu-Scott, K., & Lee, C. M. (2017). Cascading off the west Greenland shelf: A numerical perspective. *Journal of Geophysical Research: Oceans*, 122(7), 5316–5328. <https://doi.org/10.1002/2017JC012801>
- Masina, S., Storto, A., Ferry, N., Valdivieso, M., Haines, K., Balmaseda, M., et al. (2017). An ensemble of eddy-permitting global ocean reanalyses from the MyOcean project. *Climate Dynamics*, 49(3), 813–841. <https://doi.org/10.1007/s00382-015-2728-5>
- Mastropole, D., Pickart, R. S., Valdimarsson, H., Våge, K., Jochumsen, K., & Girtton, J. (2017). On the hydrography of Denmark Strait. *Journal of Geophysical Research: Oceans*, 122(1), 306–321. <https://doi.org/10.1002/2016JC012007>
- Palanques, A., de Madron, X. D., Puig, P., Fabres, J., Guillén, J., Calafat, A., et al. (2006). Suspended sediment fluxes and transport processes in the Gulf of Lions submarine canyons. The role of storms and dense water cascading. *Marine Geology*, 234(1), 43–61. <https://doi.org/10.1016/j.margeo.2006.09.002>
- Pickart, R. S., Spall, M. A., Torres, D. J., Våge, K., Valdimarsson, H., Nobre, C., et al. (2017). The North Icelandic Jet and its relationship to the North Icelandic Irminger Current. *Journal of Marine Research*, 75(5), 605–639. <https://doi.org/10.1357/002224017822109505>
- Puig, P. (2017). Dense shelf water cascading and associated bedforms. In J. Guillén, J. Acosta, F. L. Chiocci, & A. Palanques (Eds.), *Atlas of bedforms in the western Mediterranean* (pp. 35–40). Springer International Publishing. https://doi.org/10.1007/978-3-319-33940-5_7

- Pusccheddu, A., Mea, M., Gambi, C., Bianchelli, S., Canals, M., Sanchez-Vidal, A., et al. (2010). Ecosystem effects of dense water formation on deep Mediterranean Sea ecosystems: An overview. *Advances in Oceanography and Limnology*, *1*, 67–83. <https://doi.org/10.1080/19475721003735765>
- Roughan, M., Schaeffer, A., & Cresswell, G. (2019). East Australian current. In J. K. Cochran, H. J. Bokuniewicz, & P. L. Yager (Eds.), *Encyclopedia of ocean sciences* (3rd ed., pp. 340–350). Academic Press. <https://doi.org/10.1016/B978-0-12-409548-9.11550-7>
- Saberli, A., Haine, T. W. N., Gelderloos, R., Femke de Jong, M., Furey, H., & Bower, A. (2020). Lagrangian perspective on the origins of Denmark Strait Overflow. *Journal of Physical Oceanography*, *50*(8), 2393–2414. <https://doi.org/10.1175/JPO-D-19-0210.1>
- Semper, S., Våge, K., Pickart, R. S., Valdimarsson, H., Torres, D. J., & Jónsson, S. (2019). The emergence of the North Icelandic Jet and its evolution from northeast Iceland to Denmark Strait. *Journal of Physical Oceanography*, *49*(10), 2499–2521. <https://doi.org/10.1175/JPO-D-19-0088.1>
- Smith, G. C., Roy, F., Mann, P., Dupont, F., Brasnett, B., Lemieux, J.-F., et al. (2014). A new atmospheric dataset for forcing ice–ocean models: Evaluation of reforecasts using the Canadian global deterministic prediction system. *Quarterly Journal of the Royal Meteorological Society*, *140*(680), 881–894. <https://doi.org/10.1002/qj.2194>
- Spall, M. A., Pedlosky, J., & Cenedese, C. (2017). Circulation induced by isolated dense water formation over closed topographic contours. *Journal of Physical Oceanography*, *47*(9), 2251–2265. <https://doi.org/10.1175/JPO-D-17-0042.1>
- Våge, K., Moore, G., Jónsson, S., & Valdimarsson, H. (2015). Water mass transformation in the Iceland Sea. *Deep Sea Research Part I: Oceanographic Research Papers*, *101*, 98–109. <https://doi.org/10.1016/j.dsr.2015.04.001>
- Våge, K., Pickart, R. S., Spall, M. A., Moore, G., Valdimarsson, H., Torres, D. J., et al. (2013). Revised circulation scheme north of the Denmark Strait. *Deep Sea Research Part I: Oceanographic Research Papers*, *79*, 20–39. <https://doi.org/10.1016/j.dsr.2013.05.007>
- Våge, K., Pickart, R. S., Spall, M. A., Valdimarsson, H., Jonsson, S., Torres, D. J., et al. (2011). Significant role of the North Icelandic Jet in the formation of Denmark Strait overflow water. *Nature Geoscience*, *4*, 723–727. <https://doi.org/10.1038/ngeo1234>
- Vidal, A. S., Pasqual, C., Kerhervé, P., Heussner, S., Calafat, A., Palanques, A., et al. (2009). Across margin export of organic matter by cascading events traced by stable isotopes, northwestern Mediterranean Sea. *Limnology and Oceanography*, *54*(5), 1488–1500. <https://doi.org/10.4319/lo.2009.54.5.1488>
- Wobus, F., Shapiro, G. I., Huthnance, J. M., & Maqueda, M. A. (2013). The piercing of the Atlantic Layer by an Arctic shelf water cascade in an idealised study inspired by the Storfjorden overflow in Svalbard. *Ocean Modelling*, *71*, 54–65. <https://doi.org/10.1016/j.ocemod.2013.03.003>
- Ypma, S., Brüggemann, N., Georgiou, S., Spence, P., Dijkstra, H., Pietrzak, J., & Katsman, C. (2019). Pathways and watermass transformation of Atlantic Water entering the Nordic Seas through Denmark Strait in two high resolution ocean models. *Deep Sea Research Part I: Oceanographic Research Papers*, *145*, 59–72. <https://doi.org/10.1016/j.dsr.2019.02.002>